Supporting Information

Catalytic Acceptorless Dehydrogenation of Alcohols

Using Cobalt(I) Pincer Complexes Supported by P-GeH-P Ligands

Yu-Chao Liu, Dun-Xu Cao, Qi-Yang Ban, Wen-Jie Ma, and Bin Xiao*

Department of Chemistry, University of Science and Technology of China,
Hefei 230026, P. R. China.
E-mail: binxiao@ustc.edu.cn,

Table of Contents

1. General considerations

All preparations and manipulations were carried out using standard Schlenk and glovebox techniques, under an atmosphere of argon and high-purity nitrogen, respectively. All reagents were purchased from commercial sources and used without further purification unless otherwise noted. Toluene (C_7H_8), THF (C_4H_8O), and diethyl ether ($(CH_3CH_2)_2O$) were distilled under nitrogen over sodium. Dichloromethane (CH_2Cl_2) and methanol (MeOH) were dried using 3Å molecular sieves.

^{1}H-NMR spectra were recorded on 400 MHz or 500 MHz spectrometers. Chemical shifts for ^{1}H-NMR spectra are reported in parts per million (ppm) relative to tetramethylsilane ($\delta = 0$). Data for ^{1}H-NMR are presented as follows: chemical shift (δ ppm), multiplicity, coupling constant (Hz), and integration. ^{13}C-NMR spectra were recorded on 101 MHz spectrometers. Chemical shifts are reported in ppm relative to the solvent resonance as the internal standard ($CDCl_3$, δ 77.2 ppm; CD_2Cl_2, δ 53.4 ppm). Data for ^{13}C-NMR are presented in terms of chemical shift (δ ppm), multiplicity, and coupling constant (Hz). High-resolution mass spectra (HRMS) were recorded on an Acquity UPLC-Xevo G2 QTof instrument in ESI mode, unless otherwise stated. Gas chromatography (GC) analysis was performed on a Shimadzu GC-2014 Series system equipped with a flame-ionization detector. Infrared spectra were recorded using a Thermo Fisher Scientific Nicolet iS5 spectrometer equipped with an ATR accessory. Elemental analysis was determined by the vario EL cube V2.0.3 (C, H, N mode). Organic solutions were concentrated under reduced pressure using a Buchi rotary evaporator. Chromatographic purification of products was achieved through column chromatography or preparative TLC (thin-layer chromatography) on silica gel.

2. Synthesis and characterization of new compounds

2.1 P^{Ph}-GeH_2-P^{Ph} (**compound 3**)

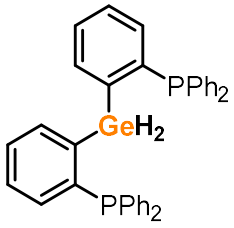

3

In a 250 mL pressure-resistant Schlenk flask, compound 1 (6.824 g, 20 mmol) was dissolved in anhydrous ether (50 mL). n-Butyllithium (1.1 equiv., 2.4 M in n-hexane, 9.2 mL) was added dropwise over a period of more than 30 minutes at -78 ºC. After the addition, the temperature was slowly raised to room temperature. After one hour at room temperature, the reaction mixture was left undisturbed to allow complete settling. Under an inert atmosphere, the supernatant was carefully removed. Anhydrous toluene (30 mL) was then added as the new solvent, and the temperature was subsequently lowered back to -78 ºC, and germanium tetrachloride (0.5 equiv., 10 mmol, 1.2 mL) was added slowly. After the addition, the temperature was slowly raised to 120 °C. The reaction was allowed to proceed for 12 hours, and then cooled to room temperature. The reaction mixture was filtered, and the filtrate was concentrated under reduced pressure. n-Hexane (about 20 mL) was added, and a large amount of white solid was precipitated (P-$GeCl_2$-P). P-$GeCl_2$-P was dissolved in a mixture of anhydrous ether and anhydrous THF (Et_2O:THF = 2:1), and $LiAlH_4$ (3 equiv., 30 mmol, 1.138g) was added. After 12 hours at room temperature, the reaction was carefully quenched by dropwise addition of water (10 mL) at 0 °C (ice-water bath) until no further gas evolution was observed. The mixture was filtered, and the filtrate was extracted with ethyl acetate (3 * 10 mL). The combined organic phases were dried over anhydrous Na_2SO_4 and concentrated under reduced pressure. The product was purified by silica gel column chromatography (100-200 mesh) using petroleum ether as the eluent, and concentrated under vacuum to give a white powder with a yield of 56% (6.7 g). The white powder was dissolved in anhydrous THF, and slow evaporation yielded crystals suitable for single-crystal X-ray diffraction analysis, revealing the structure as P^{Ph}-GeH_2-P^{Ph} (**compound 3**).

^{1}H NMR (400 MHz, $CDCl_3$) δ 7.55 (dt, J = 6.9, 2.3 Hz, 2H), 7.27 (q, J = 2.0, 1.3 Hz, 9H), 7.24 – 7.23 (m, 3H), 7.16 (tt, J = 6.0, 1.9 Hz, 9H), 7.05 (ddd, J = 7.3, 3.7, 1.5 Hz, 2H), 5.43 (t, J = 8.1 Hz, 2H).

^{31}P NMR (162 MHz, $CDCl_3$) δ -8.45.

^{13}C NMR (101 MHz, $CDCl_3$) δ 142.67, 142.60, 136.20, 136.18, 136.15, 136.08, 136.06, 132.62,

132.55, 132.47, 128.35, 127.46, 127.27, 127.22.

HRMS (ESI) m/z ($[M+H]^+$) Calcd for $[C_{36}H_{30}GeP_2+H]^+$: 599.1113; Found: 599.1168.

2.2 Co{κ^3*P,Ge,P*-(P^{Ph}-GeH-P^{Ph})$(CO)_2$} (**compound 4**)

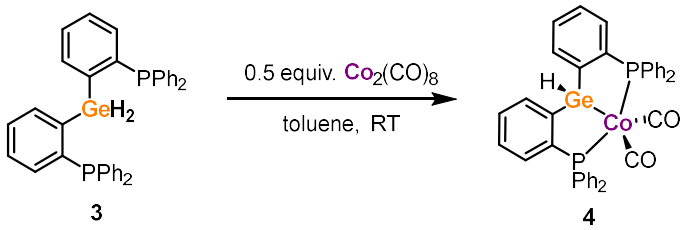

In a 25 mL Schlenk tube, compound 3 (597.2 mg, 1 mmol) was added and dissolved in anhydrous toluene (2 mL). A solution of $Co_2(CO)_8$ (0.5 equiv., 0.5 mmol) in anhydrous toluene (2 mL) was slowly added. After the addition was complete, the mixture was stirred at room temperature for 1 hour, during which the solution gradually turned reddish-brown. Hexane (about 10 mL) was added, precipitating a large amount of light yellow solid. The solid was filtered and then redissolved in an appropriate amount of dichloromethane (about 1 mL). Methanol (about 0.5 mL) was slowly added, resulting in the precipitation of light yellow crystals. No further purification was needed, yielding 92% (654.1 mg).

Anal. Calcd. for $C_{38}H_{29}CoGeO_2P_2$: C, 64.18; H, 4.11; O, 4.50; N 0.00. **Found:** C, 63.67; H, 4.22; N 0.00.

^{1}H NMR (500 MHz, CD_2Cl_2) δ 8.01 (d, *J* = 7.3 Hz, 2H), 7.73 (s, 4H), 7.41 (d, *J* = 21.5 Hz, 9H), 7.24 (d, *J* = 11.0 Hz, 4H), 7.17 (d, *J* = 7.6 Hz, 2H), 6.96 (t, *J* = 7.6 Hz, 5H), 6.57 (s, 4H), 5.96 (s, 1H).

^{31}P NMR (202 MHz, CD_2Cl_2) δ 79.01.

^{13}C NMR (101 MHz, CD_2Cl_2) δ 216.6, 206.1, 154.8, 154.4, 154.1, 144.1, 143.8, 143.6, 139.6, 139.4, 139.1, 138.7, 138.5, 138.3, 133.2, 133.2, 133.1, 133.0, 132.9, 131.6, 131.4, 131.3, 131.2, 130.2, 130.0, 128.7, 128.6, 128.5, 128.5, 128.4, 128.4.

HRMS (ESI) m/z ($[M+Na]^+$) Calcd for $[C_{38}H_{29}CoGeO_2P_2+Na]^+$: 735.0084; Found: 735.0062.

ATR-IR: ν(Co-CO) 1973cm^{-1}, 1917cm^{-1}.

2.3 Co{κ^3*P,Ge,P*-(P^{Ph}-GeCl-P^{Ph})$(CO)_2$} (**compound 5**)

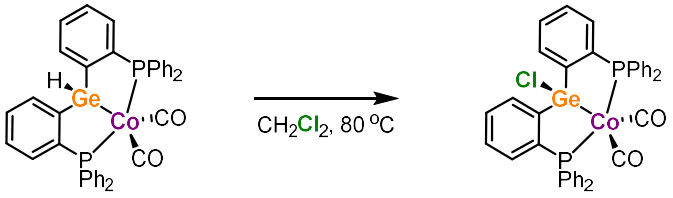

4 **5**

In a 10 mL Schlenk tube, compound 4 (711.2 mg, 1 mmol) were added, followed by 2 mL of dichloromethane. The reaction was carried out at 80 ºC for 2 hours, after which it was cooled to room temperature. Methanol (about 2 mL) was slowly added to the reaction mixture, resulting in the precipitation of light yellow crystals. No further purification was required, yielding 93% (693.4 mg).

Anal. Calcd. for $C_{36}H_{28}ClCoGeO_2P_2$: C, 61.21; H, 3.79; O, 4.29; N 0.00. **Found:** C, 61.16; H, 3.89; N 0.13.

1H NMR (500 MHz, $CDCl_3$) δ 8.15 (d, J = 7.4 Hz, 2H), 7.72 (tt, J = 6.0, 3.2 Hz, 4H), 7.53 (t, J = 7.4 Hz, 2H), 7.43-7.33 (m, 8H), 7.30 (t, J = 7.4 Hz, 2H), 7.17 (t, J = 7.4 Hz, 2H), 6.96 (t, J = 7.6 Hz, 4H), 6.66 (q, J = 6.1 Hz, 4H).

^{31}P NMR (162 MHz, $CDCl_3$) δ 79.15.

^{13}C NMR (101 MHz, CD_2Cl_2) δ 215.2, 203.5, 156.8, 156.5, 156.1, 141.8, 141.5, 141.3, 138.6, 138.4, 138.1, 137.4, 137.2, 137.0, 133.0, 132.9, 132.9, 132.3, 132.2, 132.0, 131.5, 131.5, 131.4, 131.3, 130.4, 130.0, 130.0, 129.9, 129.3, 128.9, 128.8, 128.8, 128.7, 128.7.

HRMS (ESI) m/z ($[M+Na]^+$) Calcd for $[C_{36}H_{28}ClCoGeO_2P_2+Na]^+$: 768.9695; Found: 768.9721.

ATR-IR: ν(Co-CO) 1981cm^{-1}, 1934cm^{-1}.

2.4 Co{κ^3*P,Ge,P*-(P^{Ph}-GeMe-P^{Ph})$(CO)_2$} (**compound 6**)

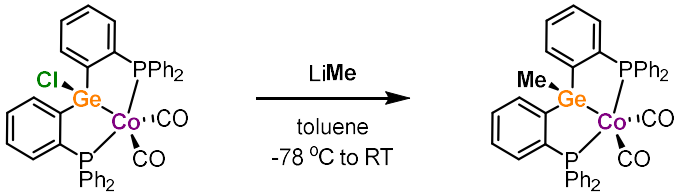

5 **6**

In a 10 mL Schlenk tube, compound 5 (149.2 mg, 0.2 mmol) was added and dissolved in 1 mL of anhydrous toluene. At -78 °C, a solution of methyl lithium (1.2 equiv., 1.6 M in Et_2O, 0.15 mL) was slowly added dropwise. After the addition was complete, the temperature was gradually raised to room temperature. The reaction was allowed to proceed at room temperature for 2 hours, after which the reaction mixture was concentrated under reduced pressure. The residue was redissolved in dichloromethane (about 1 mL), and methanol (about 0.5 mL) was slowly added, resulting in the precipitation of light yellow crystals. No further purification was necessary, yielding 76% (110.2 mg).

Anal. Calcd. for $C_{39}H_{31}CoGeO_2P_2$: C, 64.59; H, 4.31; O, 4.41; N 0.00. **Found:** C, 63.72; H, 4.32; N 0.07.

^{1}H NMR (400 MHz, $CDCl_3$) δ 8.08 (d, *J* = 7.3 Hz, 2H), 7.75 (s, 4H), 7.49 (d, *J* = 8.1 Hz, 2H), 7.33 (d, *J* = 25.5 Hz, 10H), 7.15 (t, *J* = 7.7 Hz, 2H), 6.93 (t, *J* = 7.7 Hz, 4H), 6.61 (s, 4H), 3.33 (s, 3H).

^{31}P NMR (162 MHz, $CDCl_3$) δ 80.64.

^{13}C NMR (101 MHz, $CDCl_3$) δ 215.7, 203.1, 155.1, 154.7, 154.4, 142.7, 142.4, 142.2, 139.0, 138.8, 138.6, 137.9, 137.7, 137.5, 133.0, 132.8, 132.8, 132.7, 132.0, 131.9, 131.7, 131.3, 131.1, 131.0, 131.0, 130.3, 129.7, 129.5, 129.2, 128.4, 128.3, 128.2, 128.2, 128.1, 53.3.

HRMS (ESI) m/z ($[M+H]^+$) Calcd for $[C_{39}H_{31}CoGeO_2P_2+H]^+$: 727.0421; Found: 727.0464.

ATR-IR: ν(Co-CO) 1989cm^{-1}, 1949cm^{-1}.

2.5 Co{κ^3*P,Si,P*-(P^{Ph}-SiH-P^{Ph})$(CO)_2$}

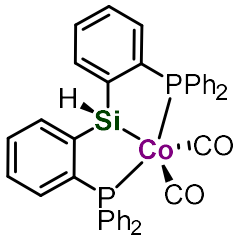

Referring to previous work[1], the silicon analogue of H-Ge-Co was synthesized, and its characterization is as follows:

^{1}H NMR (400 MHz, CD_2Cl_2) δ 8.03 (d, *J* = 7.4 Hz, 2H), 7.74 (tt, *J* = 6.3, 3.1 Hz, 4H), 7.45 (t, *J* = 7.3 Hz, 2H), 7.41 – 7.36 (m, 6H), 7.32 – 7.23 (m, 4H), 7.16 (t, *J* = 7.4 Hz, 2H), 6.93 (t, *J* = 7.6 Hz, 4H), 6.61 – 6.53 (m, 4H), 5.75 (s, 1H).

^{31}P NMR (162 MHz, CD_2Cl_2) δ 74.30.

^{13}C NMR (101 MHz, CD_2Cl_2) δ 152.2, 151.8, 151.5, 146.5, 146.2, 146.0, 139.2, 139.0, 138.8, 138.0, 137.8, 137.6, 133.1, 133.0, 132.9, 132.9, 132.8, 132.7, 130.8, 130.8, 130.7, 129.8, 129.7, 128.5, 128.5, 128.5, 128.3, 128.2, 128.2, 128.1, 128.1. The resonance of the carbonyl carbons could not be detected.

3. General procedure for catalytic dehydrogenation reaction

3.1 General procedure for catalytic dehydrogenation reaction of 1-phenylethanol

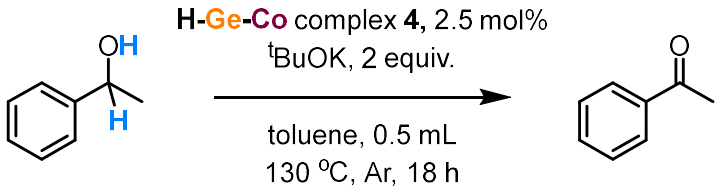

Entry	*deviation from standard condtions*	*yield (%)[b]*
1	none	86
2	without **H-Ge-Co** complex **4**	trace
3	without **KO^{t}Bu**	trace
4	**KOTMS** instead of **KO^{t}Bu**	20
5	**K_2CO_3** instead of **KO^{t}Bu**	trace
6	**n-hexane** instead of **toluene**	95
7	free ligand **3** instead of **4**	trace
8	$Co_2(CO)_8$ instead of **4**	7
9	**H-Si-Co** complex analogue instead of ***4***	trace

Scheme S1. Dehydrogenation of 1-phenylethanol catalyzed by **H-Ge-Co** complex

In a 10 mL Schlenk tube, complex catalyst and base were sequentially added, followed by 0.5 mL of solvent, and finally 1-phenylethanol (0.2 mmol). The reaction was carried out at 130 °C for 18 hours. After the reaction was completed, the mixture was cooled to room temperature and quenched with water. Propylbenzene was added as an internal standard, and the supernatant was taken for analysis by GC.

3.2 Dehydrogenation of 1-phenylethanol catalyzed by H-Si-Co complex instead of H-Ge-Co

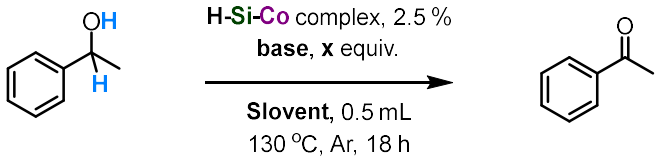

Entry	*x*	*base*	*Solvent*	*yield (%)*
1	2	^{t}BuOK	toluene	trace
2	0	^{t}BuOK	toluene	trace
3	0.1	^{t}BuOK	toluene	trace
4	0.5	^{t}BuOK	toluene	trace
5	2	^{t}BuOK	n-hexane	trace
6	0	^{t}BuOK	n-hexane	trace
7	2	KOTMS	toluene	trace
8	2	K_2CO_3	toluene	trace

Scheme S2. Dehydrogenation of 1-phenylethanol catalyzed by **H-Si-Co** complex

3.3 General procedure for the synthesis of 2-quinolone derivatives.

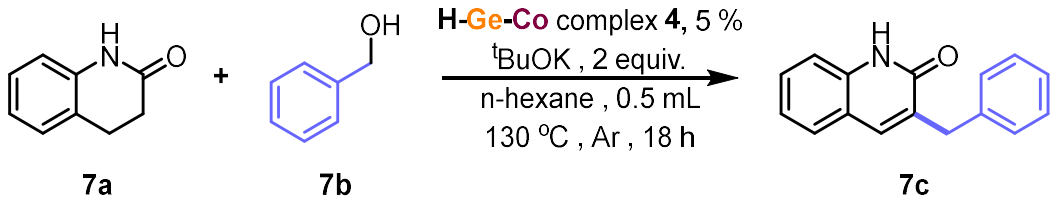

7a **7b** **7c**

In a 10 mL Schlenk tube, 7a (0.1 mmol, 14.7 mg), H-Ge-Co compound 4 (3.5 mg, 5 mol%), and KOtBu (2 equiv., 22.4 mg) were sequentially added, followed by 0.5 mL of n-hexane, and finally benzyl alcohol (0.2 mmol, 21 μL). The reaction was carried out at 130 °C for 18 hours. After the reaction was completed, the mixture was cooled to room temperature and quenched with water. The mixture was then extracted, separated, dried, filtered, and concentrated under reduced pressure. Subsequently, purification was performed using silica gel column chromatography (100–200 mesh) with an eluent (Petroleum ether : Ethyl acetate = 1:1), and the product was concentrated under vacuum to yield a white powder with a yield of 81%. The characterization results were consistent with those reported in the previous literature[2].

4. Hydrogen gas measurement and kinetic studies

4.1 Hydrogen Collection and Quantitative Detection

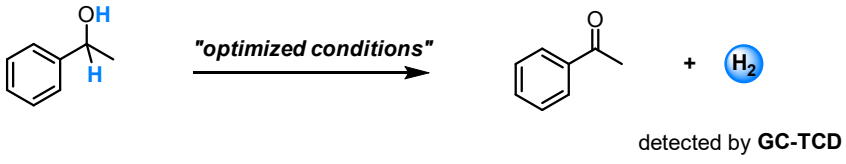

$n(H_2)$ = 0.20 mmol **[theoretical]**
$n(H_2)$ = 0.19 mmol **[measured]**

Hydrogen collection system ⟹

Scheme S3. Hydrogen collection system

By using a specially designed Schlenk tube with dual sidearms, the generated gas can be collected into a gas bag with minimal loss through inert gas purging after the reaction is completed. Subsequently, the hydrogen (H_2) yield is quantitatively detected by gas chromatography (GC), which closely matches the theoretical value. This confirms that the reaction indeed proceeds via an acceptorless dehydrogenation process.

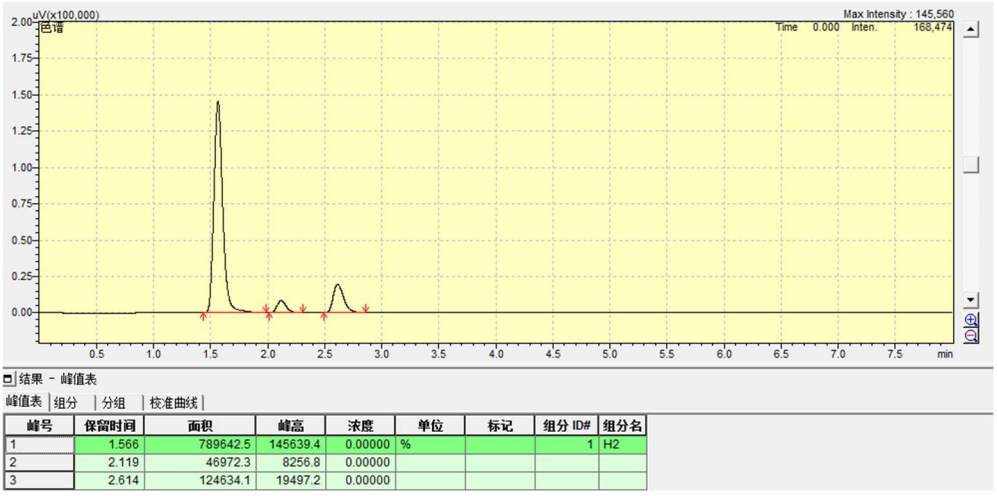

峰号	保留时间	面积	峰高	浓度	单位	标记	组分 ID#	组分名
1	1.566	789642.5	145639.4	0.00000	%		1	H2
2	2.119	46972.3	8256.8	0.00000				
3	2.614	124634.1	19497.2	0.00000				

Figure S1. The gas chromatogram for quantitative detection of post-reaction gases

According to the previously established calibration curve of GC peak area versus known hydrogen concentrations, the hydrogen peak integration area of 789642.5 indicates that the hydrogen content collected in the 500 mL gas bag is 0.91%. Based on the molar volume of gas

at room temperature (24.0 L/mol), the amount of hydrogen produced by the reaction is calculated to be 0.19 mmol.

Table S1. Hydrogen integration area versus hydrogen concentration

	Hydrogen integration area	**V%（H2）**
Calibration curve	1824131	2.108343665
Concentration to be measured	789642.5	0.912674453

4.2 Details of Kinetic Experiments

Kinetic experiments were conducted following the general procedure for the dehydrogenation of 1-phenylethanol, and the specific data are as follows:

4.2.1 Kinetic Studies on the catalyst

Table S2-1. Reaction monitoring at different catalyst concentrations

Equation	y = a + b*x				
Plot	0.5 mol% catalyst	1.0 mol% catalyst	1.5 mol% catalyst	2.0 mol% catalyst	2.5 mol% catalyst
Weight	No Weighting				
Intercept	-0.53333 ± 0.87305	1.73333 ± 0.49889	-3.2 ± 0.74833	-5.93333 ± 0.49889	-9.53333 ± 0.49889
Slope	0.17 ± 0.01347	0.26 ± 0.0077	0.42667 ± 0.01155	0.54667 ± 0.0077	0.62 ± 0.0077
Residual Sum of Squares	0.32667	0.10667	0.24	0.10667	0.10667
Pearson's r	0.99687	0.99956	0.99963	0.9999	0.99992
R-Square (COD)	0.99376	0.99912	0.99927	0.9998	0.99985
Adj. R-Square	0.98752	0.99825	0.99854	0.9996	0.99969

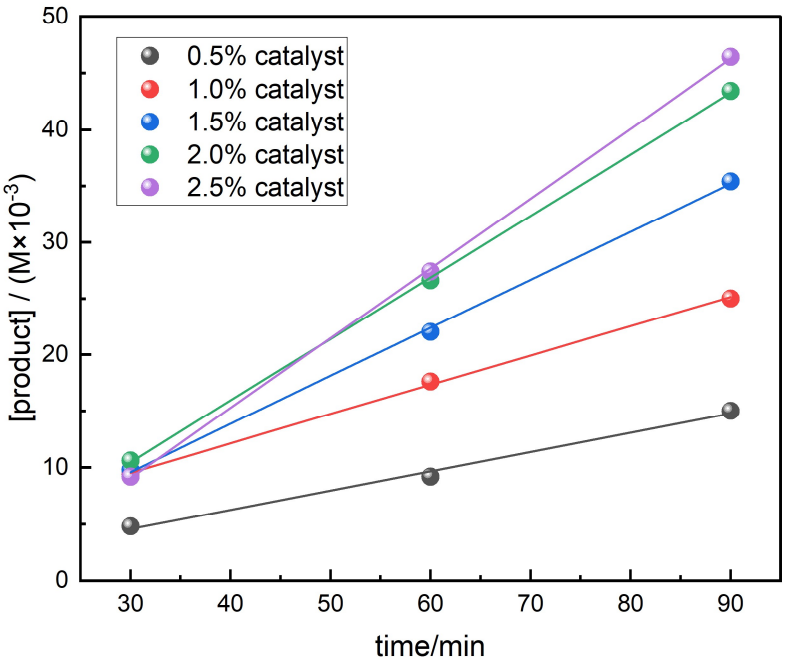

Figure S2-1. Reaction monitoring at different catalyst concentrations

Table S2-2. Kinetic order of the dehydrogenation reaction with respect to the catalyst

Equation	y = a + b*x
Plot	Reaction rate
Weight	No Weighting
Intercept	-0.04826 ± 0.00719
Slope	1.57732 ± 0.03391
Residual Sum of Squares	8.63E-05
Pearson's r	0.99931
R-Square (COD)	0.99862
Adj. R-Square	0.99815

Figure S2-2. Kinetic order of the dehydrogenation reaction with respect to the catalyst

4.2.2 Kinetic Studies on the 1-phenylethanol

Table S3-1. Reaction monitoring at different 1-phenylethanol concentrations

Equation	y = a + b*x				
Plot	0.10 mmol alcohol	0.15 mmol alcohol	0.20 mmol alcohol	0.25 mmol alcohol	0.30 mmol alcohol
Weight	No Weighting				
Intercept	-0.86667 ± 0.99778	0.46667 ± 1.24722	1.73333 ± 0.49889	-1.93333 ± 1.62138	-2.06667 ± 0.24944
Slope	0.11333 ± 0.0154	0.18667 ± 0.01925	0.26 ± 0.0077	0.35 ± 0.02502	0.42667 ± 0.00385
Residual Sum of Squares	0.42667	0.66667	0.10667	1.12667	0.02667
Pearson's r	0.9909	0.99473	0.99956	0.99745	0.99996
R-Square (COD)	0.98188	0.98948	0.99912	0.99492	0.99992
Adj. R-Square	0.96376	0.97897	0.99825	0.98983	0.99984

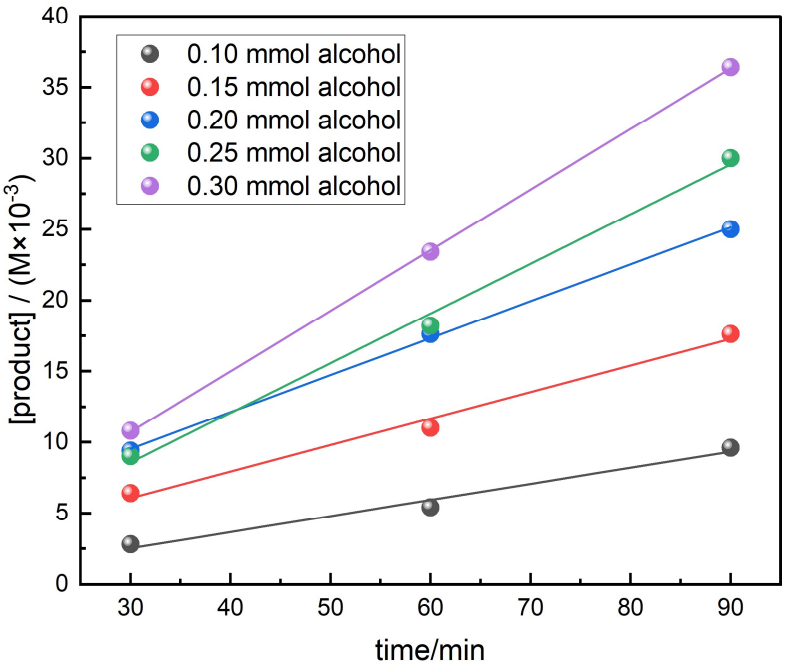

Figure S3-1. Reaction monitoring at different 1-phenylethanol concentrations

Table S3-2. Kinetic order of the dehydrogenation reaction with respect to the 1-phenylethanol

Equation	y = a + b*x
Plot	Reaction rate
Weight	No Weighting
Intercept	-0.04826 ± 0.00719
Slope	1.57732 ± 0.03391
Residual Sum of Squares	8.63E-05
Pearson's r	0.99931
R-Square (COD)	0.99862
Adj. R-Square	0.99815

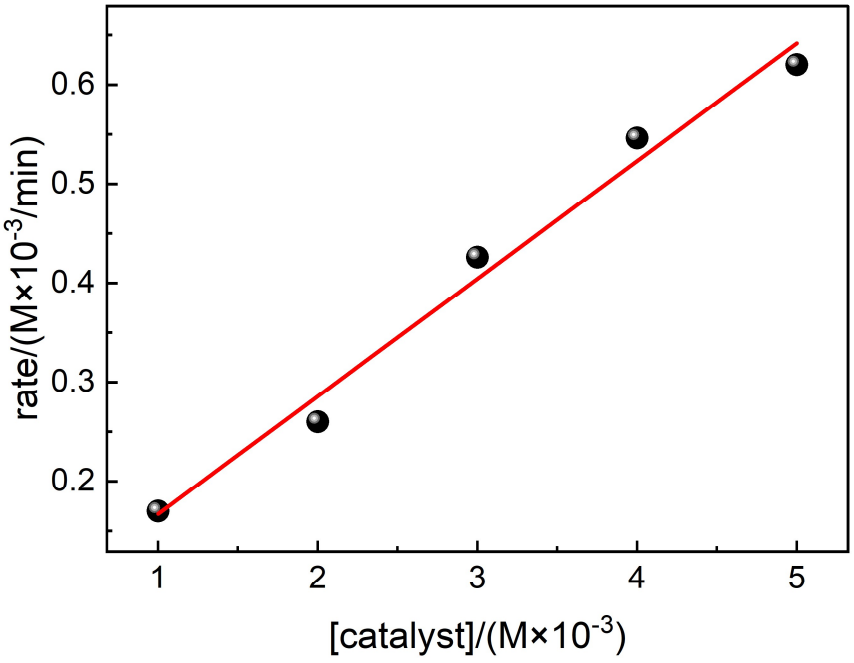

Figure S3-2. Kinetic order of the dehydrogenation reaction with respect to the 1-phenylethanol

4.2.3 Kinetic Studies on the KO^{t}Bu

Table S4-1. Reaction monitoring at different KO^{t}Bu concentrations

Equation	y = a + b*x				
Plot	1.0 equiv. KO^{t}Bu	1.5 equiv. KO^{t}Bu	2.0 equiv. KO^{t}Bu	2.5 equiv. KO^{t}Bu	3.0 equiv. KO^{t}Bu
Weight	No Weighting				
Intercept	4.86667 ± 2.12027	1.66667 ± 0.24944	1.73333 ± 0.49889	-2 ± 2.24499	-3.93333 ± 1.24722
Slope	0.27667 ± 0.03272	0.3 ± 0.00385	0.26 ± 0.0077	0.24 ± 0.03464	0.29333 ± 0.01925
Residual Sum of Squares	1.92667	0.02667	0.10667	2.16	0.66667
Pearson's r	0.99308	0.99992	0.99956	0.98974	0.99785
R-Square (COD)	0.98621	0.99984	0.99912	0.97959	0.99571
Adj. R-Square	0.97242	0.99967	0.99825	0.95918	0.99143

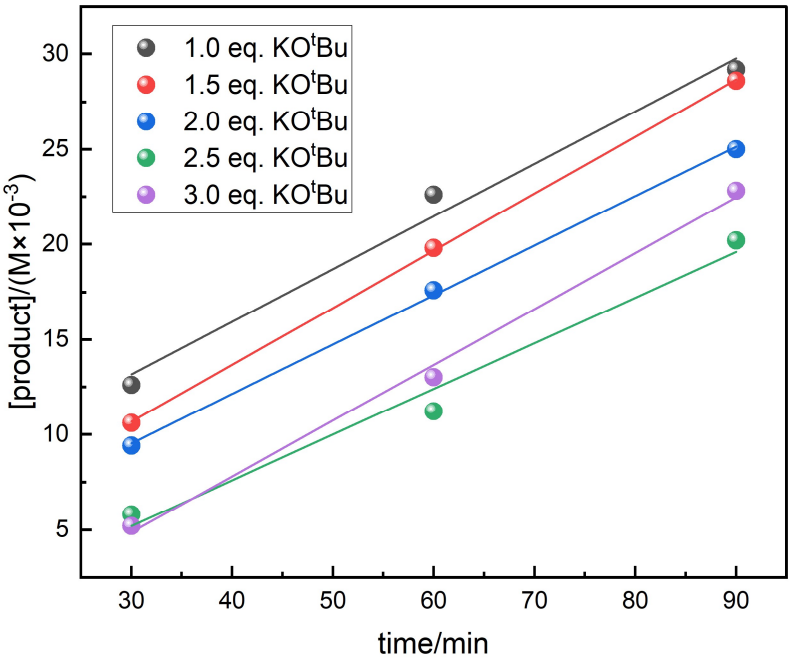

Figure S4-1. Reaction monitoring at different KO^{t}Bu concentrations

Table S4-2. Kinetic order of the dehydrogenation reaction with respect to the KO^{t}Bu

Equation	y = a + b*x
Plot	Reaction rate
Weight	No Weighting
Intercept	0.28467 ± 0.03745
Slope	-0.02668 ± 0.08827
Residual Sum of Squares	0.00234
Pearson's r	-0.1719
R-Square (COD)	0.02955
Adj. R-Square	-0.29393

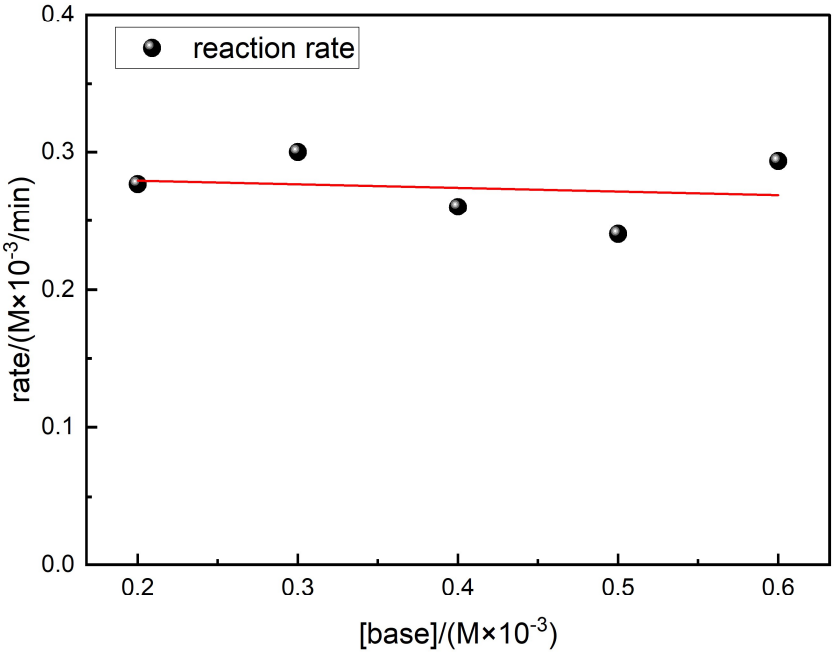

Figure S4-2. Kinetic order of the dehydrogenation reaction with respect to the KO^{t}Bu

4.2.4 Hammett Linear Free Energy Relationship (LFER) Experiment

Table S5-1. Reaction monitoring at 1-phenylethanol with different para-substituents

Equation	y = a + b*x				
Plot	-H	-CF_3	-Me	-Cl	-OMe
Weight	No Weighting				
Intercept	-0.00533 ± 0.00125	-0.01567 ± 0.00125	-0.02433 ± 0.00998	-0.04 ± 0.00748	0.001 ± 4.37022E-17
Slope	-0.00143 ± 1.9245E-5	-3E-4 ± 1.9245E-5	-0.0016 ± 1.5396E-4	-8E-4 ± 1.1547E-4	-0.002 ± 6.74339E-19
Residual Sum of Squares	6.67E-07	6.67E-07	4.27E-05	2.40E-05	8.19E-34
Pearson's r	-0.99991	-0.99795	-0.9954	-0.98974	-1
R-Square (COD)	0.99982	0.9959	0.99083	0.97959	1
Adj. R-Square	0.99964	0.9918	0.98165	0.95918	1

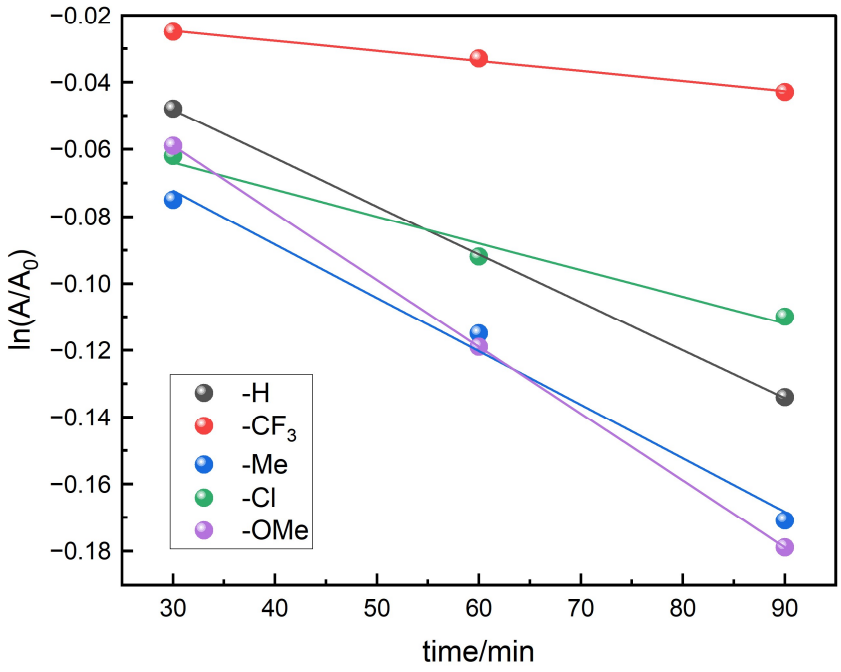

Figure S5-1. Reaction monitoring at 1-phenylethanol with different para-substituents

Table S5-2. Hammett Plot

Equation	y = a + b*x
Plot	Reaction rate
Weight	No Weighting
Intercept	-0.08117 ± 0.03372
Slope	-1.00051 ± 0.11319
Residual Sum of Squares	0.01623
Pearson's r	-0.98134
R-Square (COD)	0.96303
Adj. R-Square	0.9507

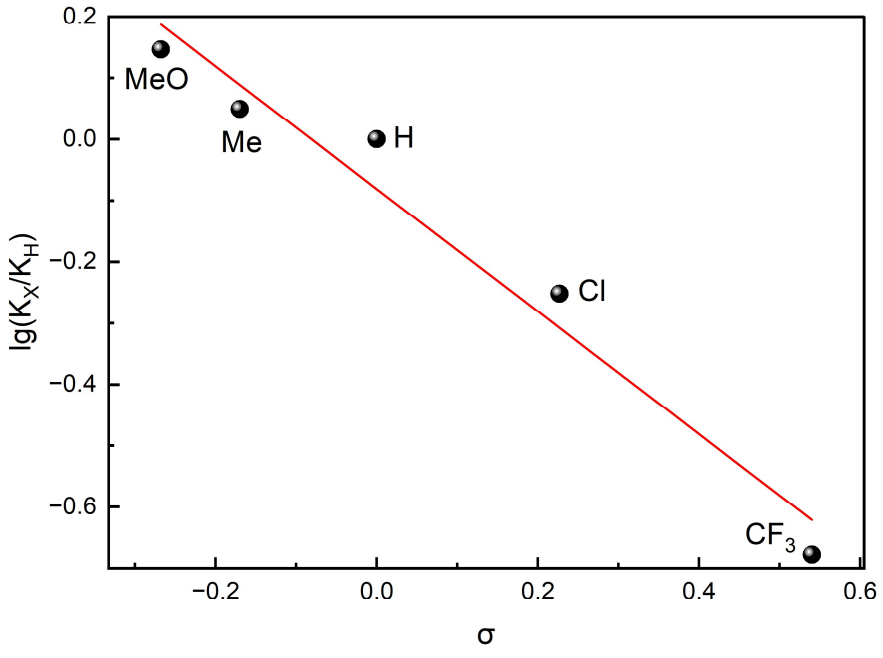

Figure S5-2. Hammett Plot

5. Hot filtration experiments

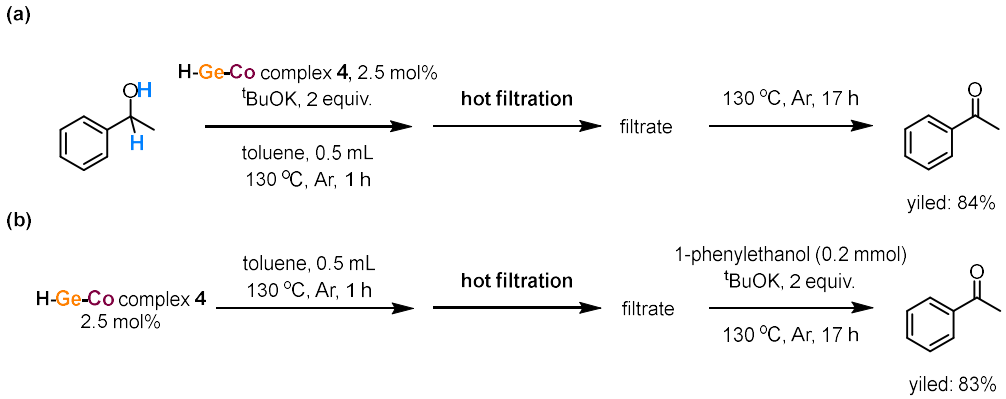

Reaction conditions:

(a) 1-phenylethanol (0.2 mmol), H-Ge-Co complex 4 (2.5 mol%), KO^{t}Bu (2 equiv.) and toluene (0.5 mL), 130 °C, under argon atmosphere for 1 hour, then rapid hot filtration at about 110 °C and stir at 130 °C for another 17 hours.

(b) H-Ge-Co complex 4 (2.5 mol%) and toluene (0.5 mL), 130 °C, under argon atmosphere for 1 hour, then rapid hot filtration at about 110 °C and add 1-phenylethanol (0.2 mmol), KO^{t}Bu (2 equiv.), stir at 130 °C for another 17 hours.

The hot-filtration test is a widely used method to determine whether metallic or nano species are responsible for substrate conversion[3]. This method involves removing metallic species by filtration at the reaction temperature and then checking whether the reaction continues in the liquid phase. In our study, the filtrate obtained from hot filtration of a heated mixture of 1-phenylethanol, base, and the cobalt catalyst still yielded 84% acetophenone. Similarly, when the cobalt catalyst alone was subjected to hot filtration and the substrate and base were added afterward, an 83% yield of acetophenone was achieved. These results suggest that our reaction system operates as a homogeneous catalytic system.

6. Proposed mechanism

To investigate the relationship between ligand structure and the catalytic performance of complexes, we substituted complex **4** with complexes **5** and **6** under the standard conditions mentioned in main text. The reactions afforded acetophenone in relatively low (36%) and moderate (50%) yields, respectively. This indicates that complex **4**, which retains the Ge-H bond, exhibits superior catalytic dehydrogenation performance compared to complex **5** (with Ge-Cl) and complex **6** (with Ge-Me).

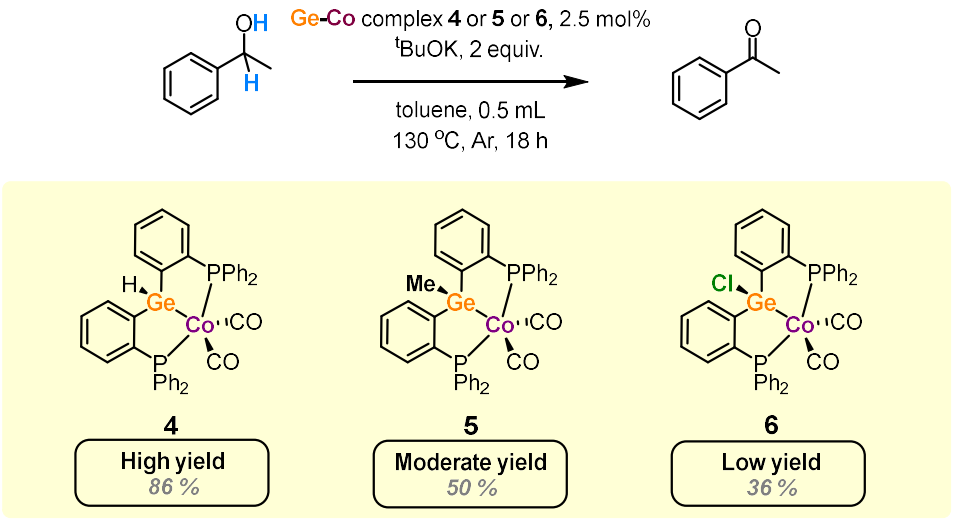

Scheme S4 Comparison of the dehydrogenation efficiency of complexes **4-6** in the acceptorless dehydrogenation of 1-phenylethanol

We speculate that this is primarily due to changes in the electron density at the cobalt center induced by the substituents. Extensive literature in this field suggests that the elimination of the benzylic hydrogen from alcohols may be involved in the rate-determining step[4]. The feasibility of this step is often closely related to the electron density of the transition metal center.

From infrared spectroscopy, we observed a gradual shift of the carbonyl absorption peaks toward higher wavenumbers—from H-Ge-Co (1973 cm^{-1}, 1917 cm^{-1}) to Me-Ge-Co (1981 cm^{-1}, 1934 cm^{-1}) and then to Cl-Ge-Co (1989 cm^{-1}, 1949 cm^{-1})—indicating a progressive decrease in the electron density at the cobalt center. This suggests a reduced ability to promote β-H elimination, which aligns with the observed decline in catalytic activity.

Note: Given the high reactivity of the Ge-Cl bond in complex **6**, we reasonably suspect that Cl-Ge-Co might not be the true active species in the catalytic cycle. An alternative explanation for the relatively lower catalytic activity of complex **6** is that Cl-Ge-Co needs to be pre-converted into the actual catalytic species H-Ge-Co to initiate the dehydrogenation cycle, which consequently leads to its diminished catalytic performance. A systematic understanding of the

catalytic activity differences among various Ge-based complexes requires both the development of more Ge-Co complex systems with diverse substituents and in-depth mechanistic investigations.

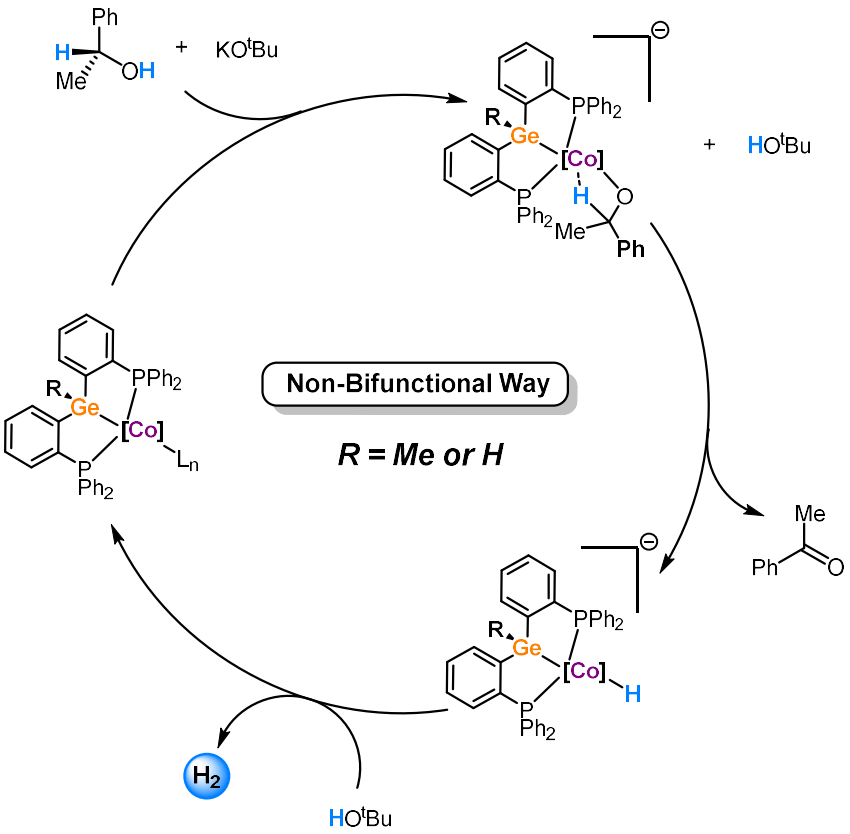

Scheme S5. Proposed mechanism

Based on previous studies of Co-catalyzed acceptorless dehydrogenation of alcohols, it is known that such reactions primarily follow two catalytic mechanisms[5]. One is the "metal-ligand cooperative" (MLC) mechanism involving non-innocent ligands, while the other is a non-bifunctional mechanism where the transition metal center directly facilitates H-elimination from the alcohol. Given the experimental observation that both H-Ge-Co and Me-Ge-Co exhibit significant catalytic activity in this work, we tend to believe that the catalytic mechanism of the Ge-Co system follows the latter.

Combined with the kinetic studies, which show first-order dependence on both the catalyst and the substrate, we have proposed the mechanistic cycle.

Note: We are fully aware that the isolation and characterization of reactive intermediates constitute crucial evidence for mechanistic studies. Therefore, the currently proposed catalytic cycle represents the most plausible interpretation based on available experimental results.

Although our attempts to isolate reaction intermediates failed to capture any Ge-H bond cleavage products, the significant reactivity demonstrated by the Ge-H bond in complex **4** prevents us from completely ruling out the possibility of a "Metal-Ligand Cooperation" (MLC) mechanism in this acceptorless dehydrogenation reaction. More sophisticated mechanistic studies and continued efforts to trap and characterize key intermediates are currently underway in our laboratory.

7. NMR spectra of compounds

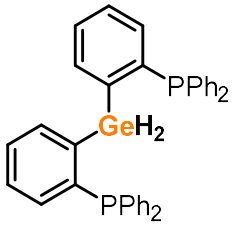

3

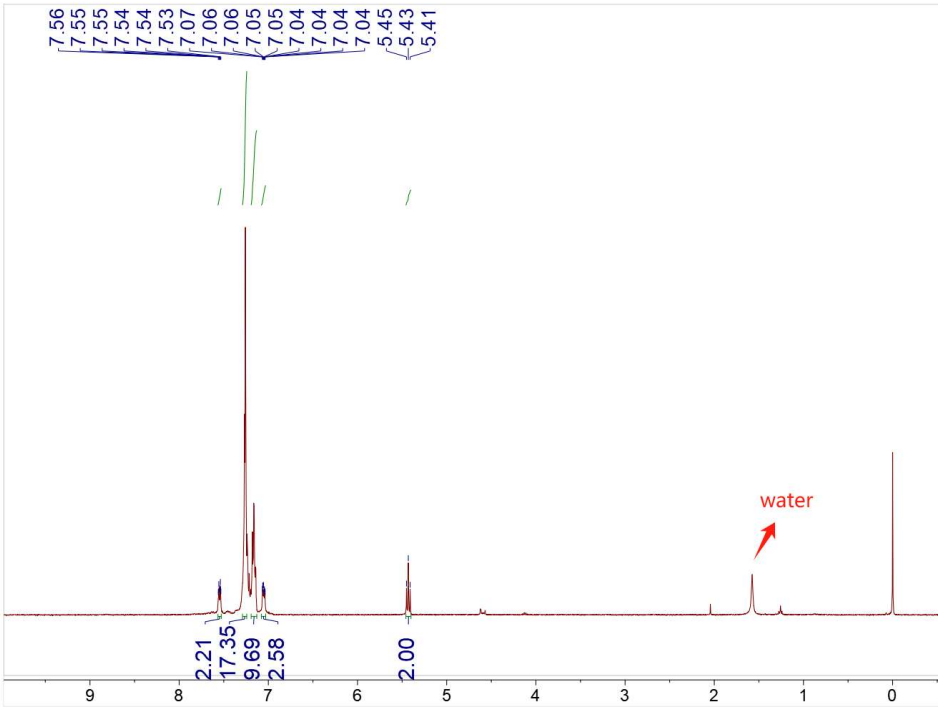

Figure S6-1. ^{1}H NMR (400 MHz, $CDCl_3$) for compound **3**.

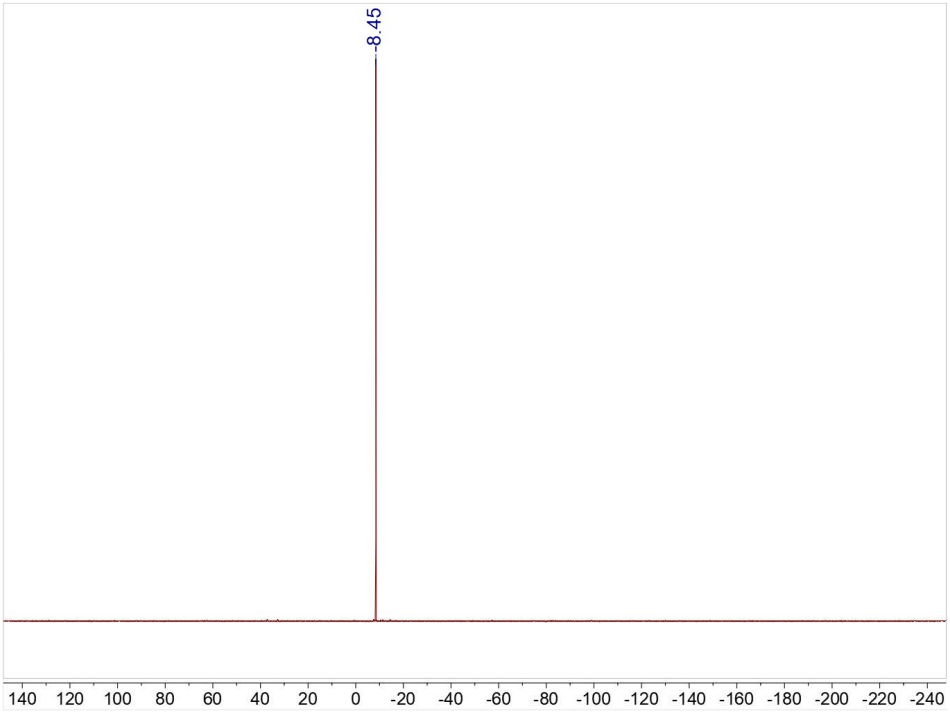

Figure S6-2. ^{31}P NMR (162 MHz, $CDCl_3$) for compound **3**.

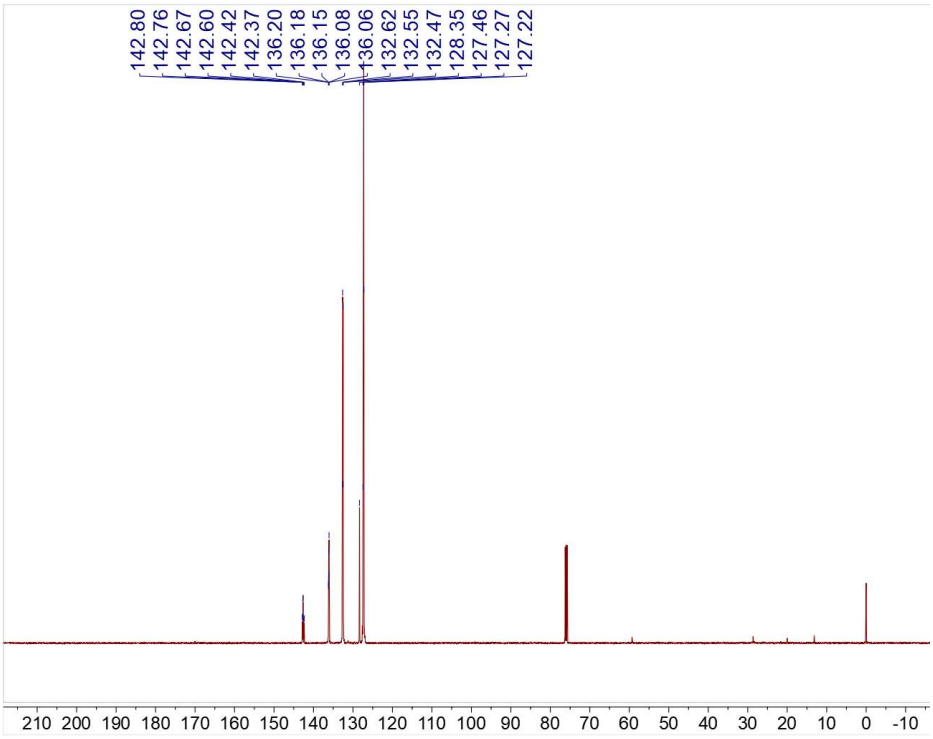

Figure S6-3. ^{13}C NMR (101 MHz, $CDCl_3$) for compound **3**.

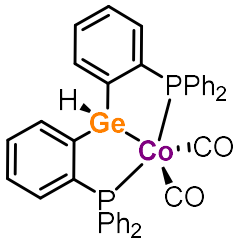

4

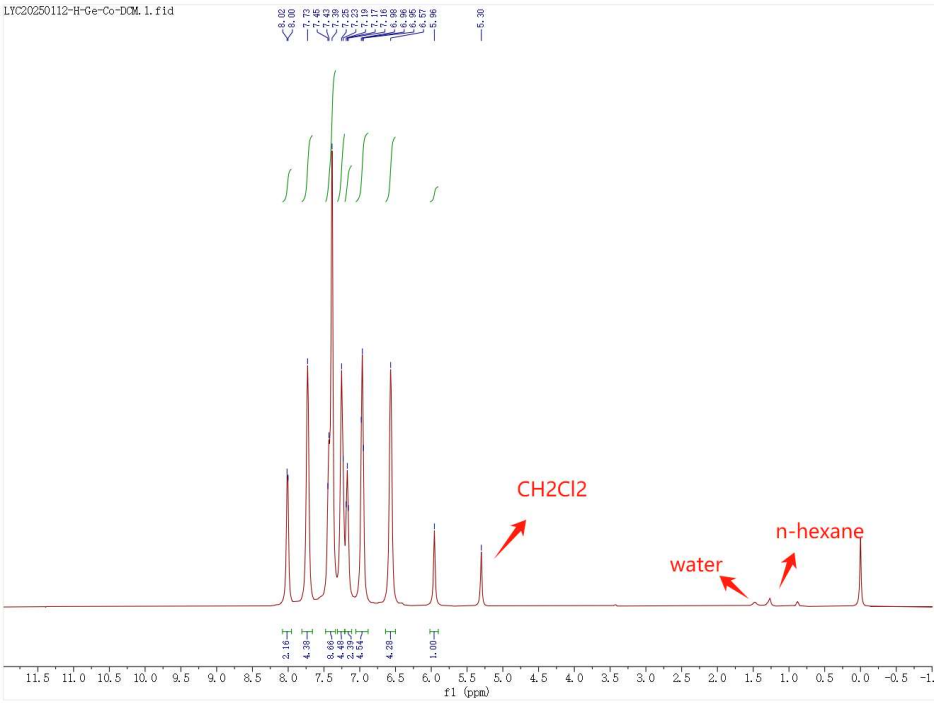

Figure S7-1. ^{1}H NMR (500 MHz, CD_2Cl_2) for compound **4**.

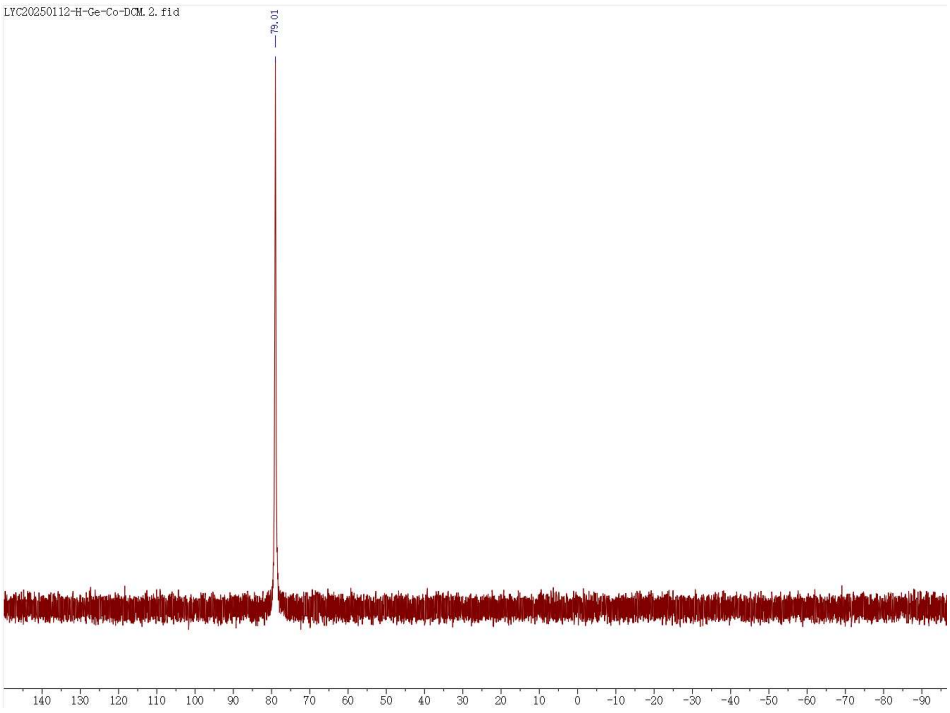

Figure S7-2. ^{31}P NMR (202 MHz, CD_2Cl_2) for compound **4**.

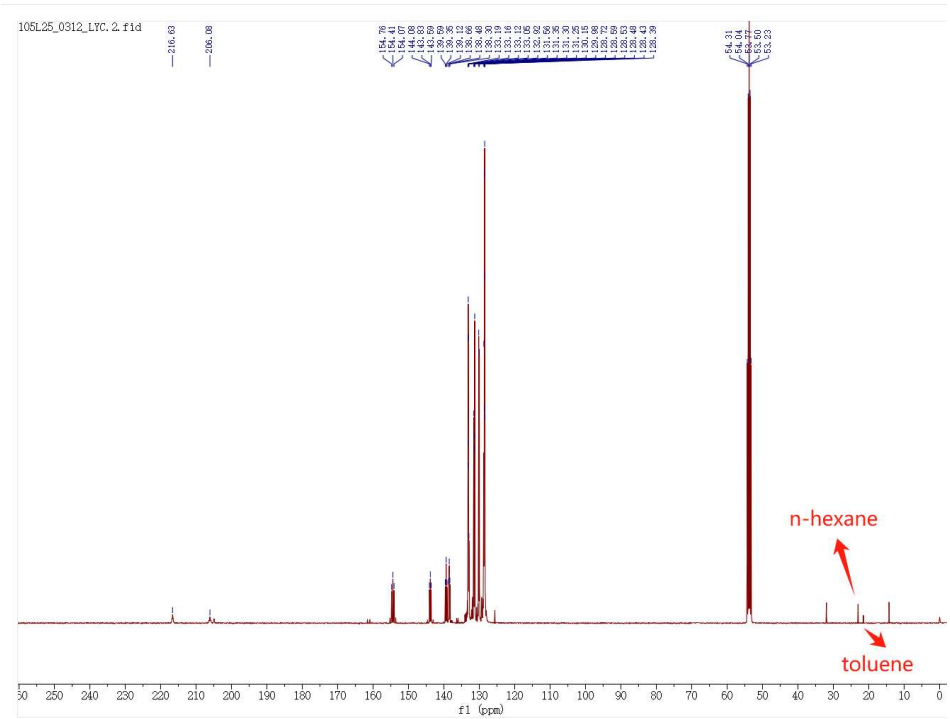

Figure S7-3. ^{13}C NMR (101 MHz, CD_2Cl_2) for compound **4**.

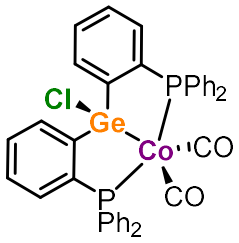

5

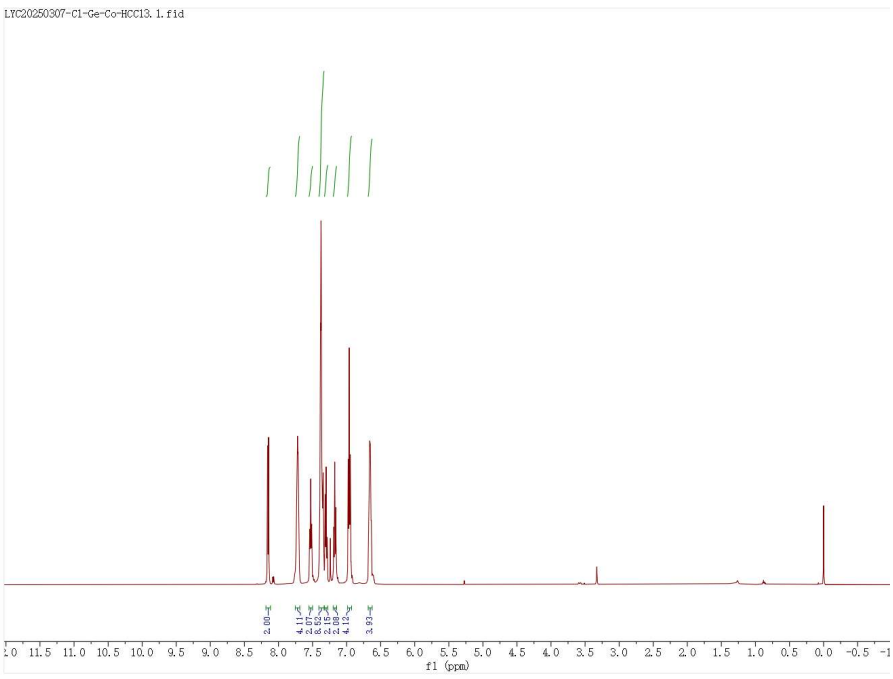

Figure S8-1. ^{1}H NMR (500 MHz, $CDCl_3$) for compound **5**.

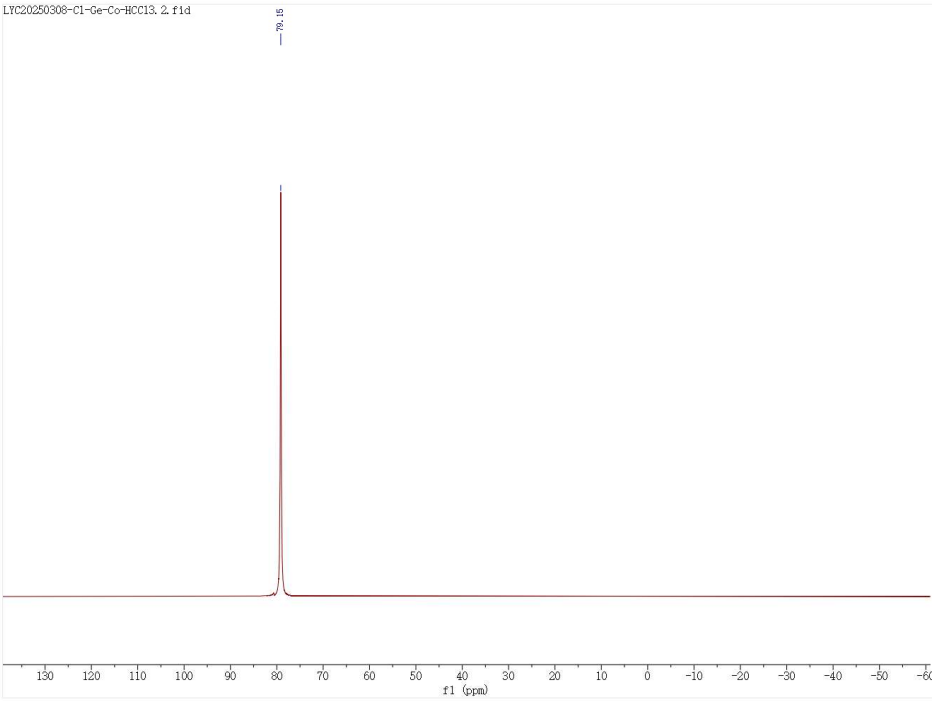

Figure S8-2. ^{31}P NMR (162 MHz, $CDCl_3$) for compound **5**.

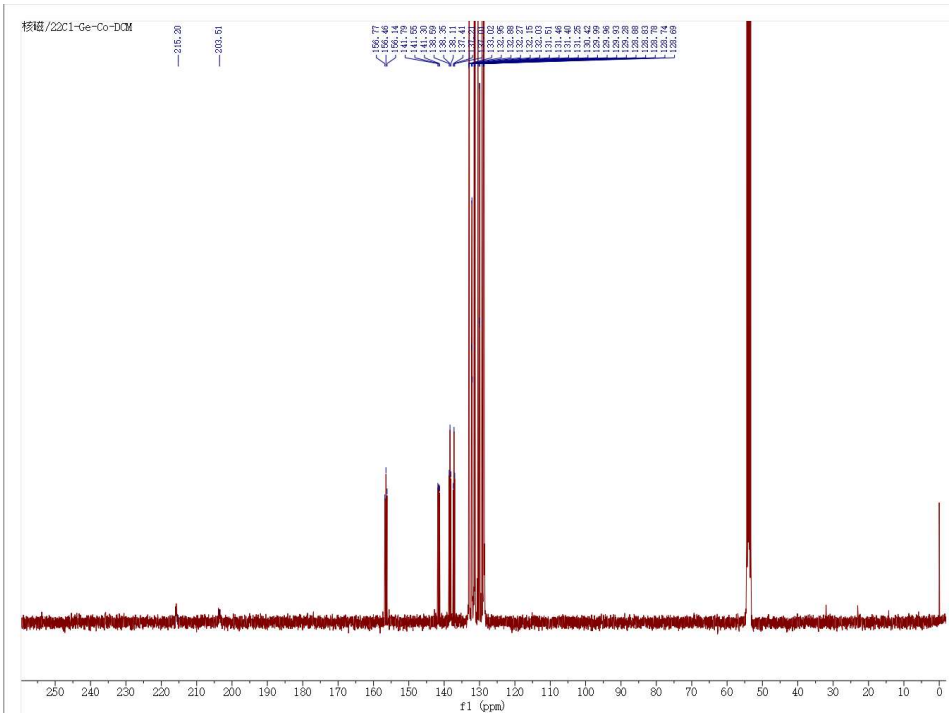

Figure S8-3. ^{13}C NMR (101 MHz, CD_2Cl_2) for compound **5**.

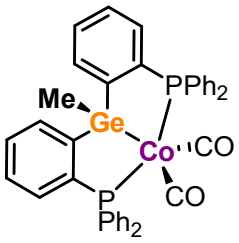

6

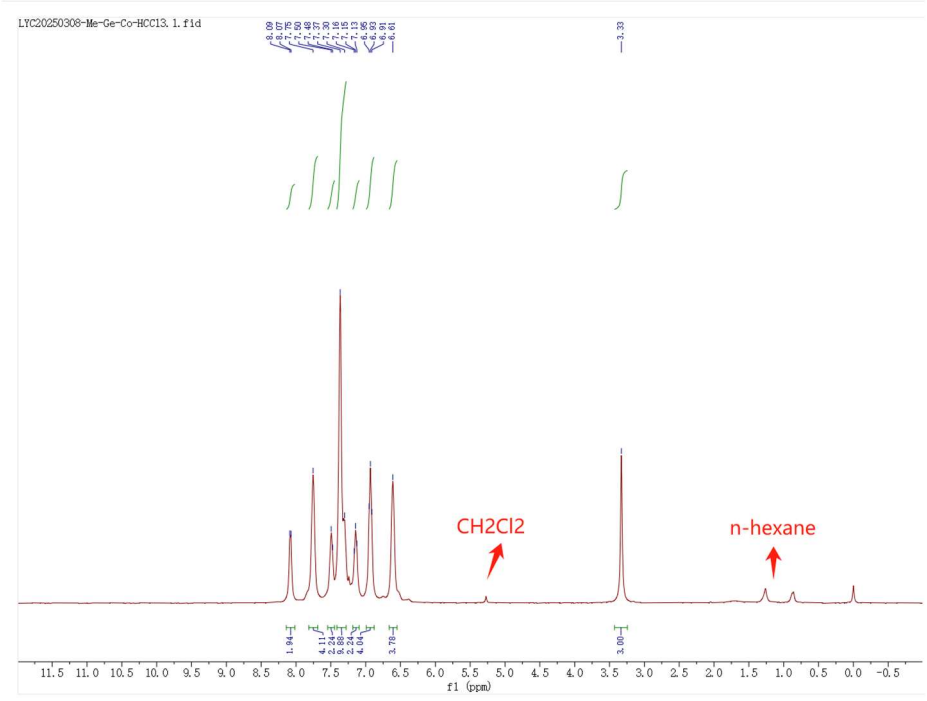

Figure S9-1. ^{1}H NMR (400 MHz, $CDCl_3$) for compound **6**.

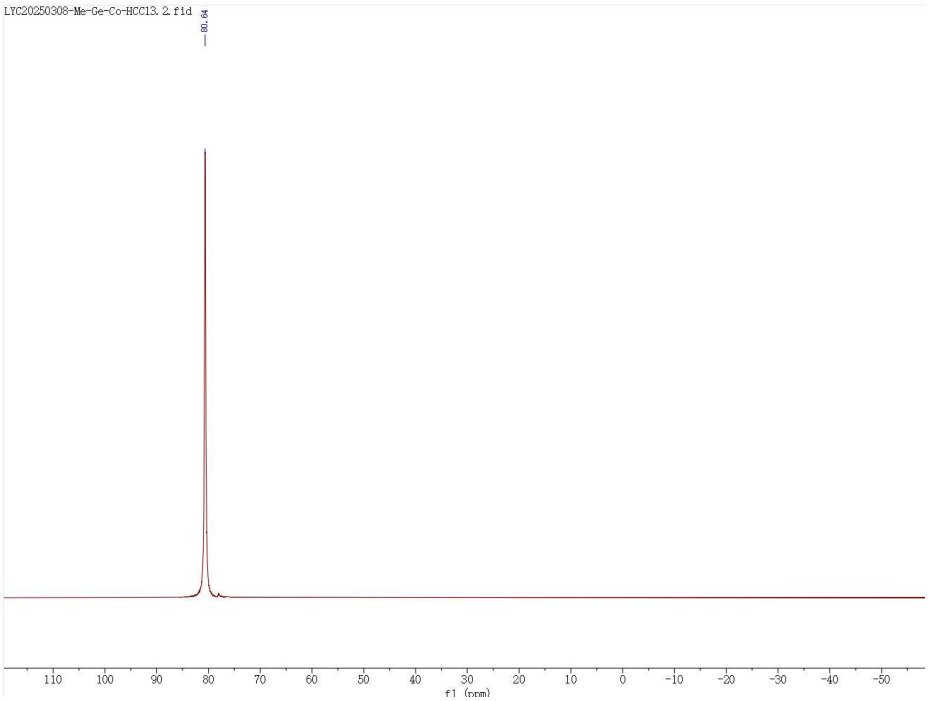

Figure S9-2. ^{31}P NMR (162 MHz, $CDCl_3$) for compound **6**.

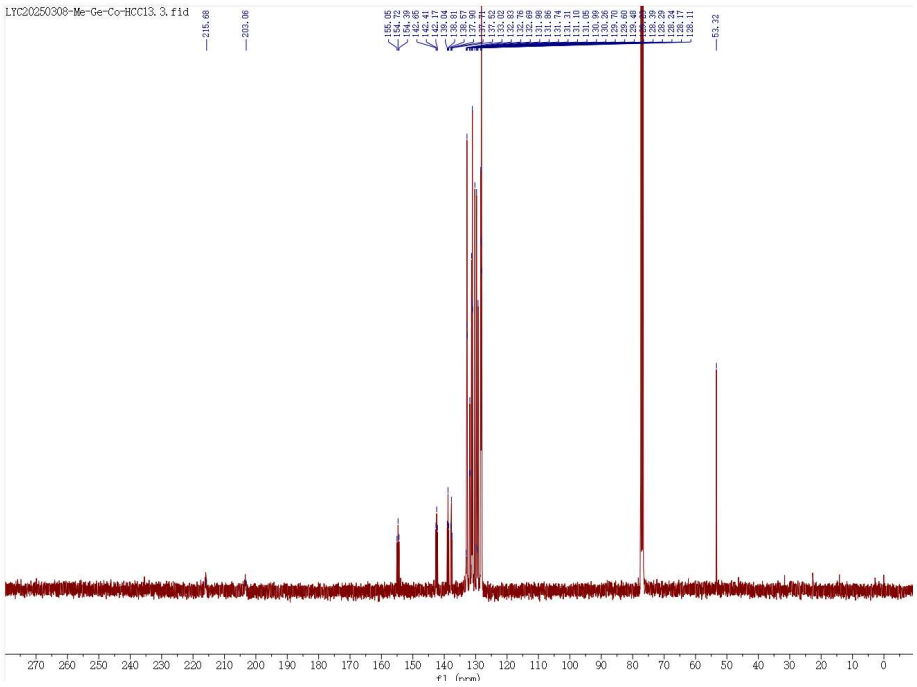

Figure S9-3. ^{13}C NMR (101 MHz, $CDCl_3$) for compound **6**.

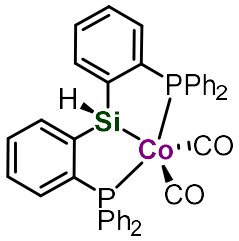

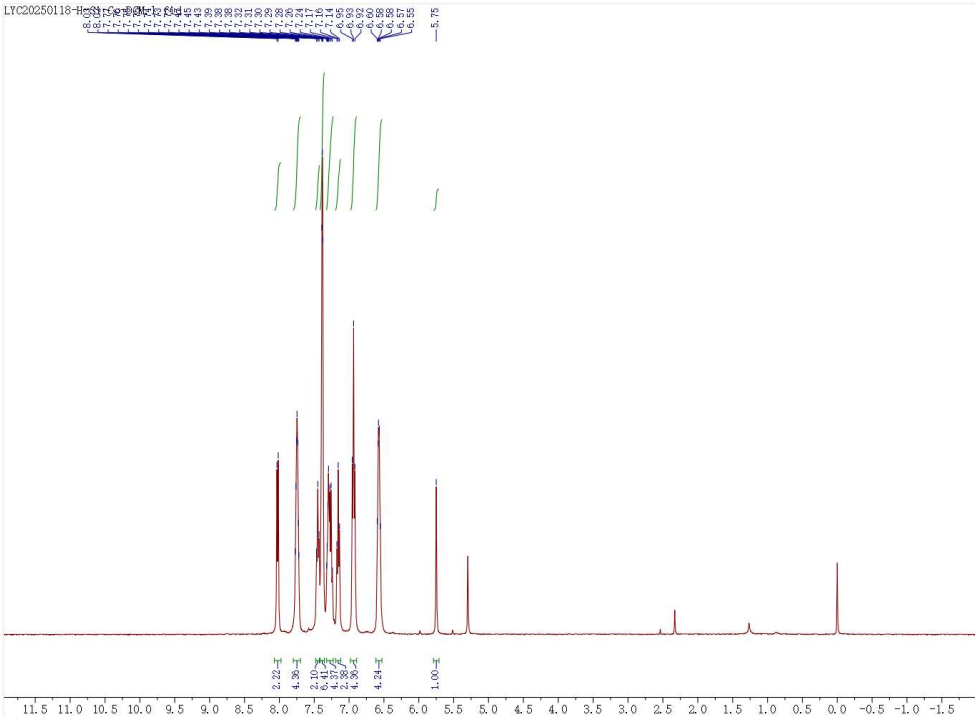

Figure S10-1. ^{1}H NMR (400 MHz, CD_2Cl_2) for compound **H-Si-Co**.

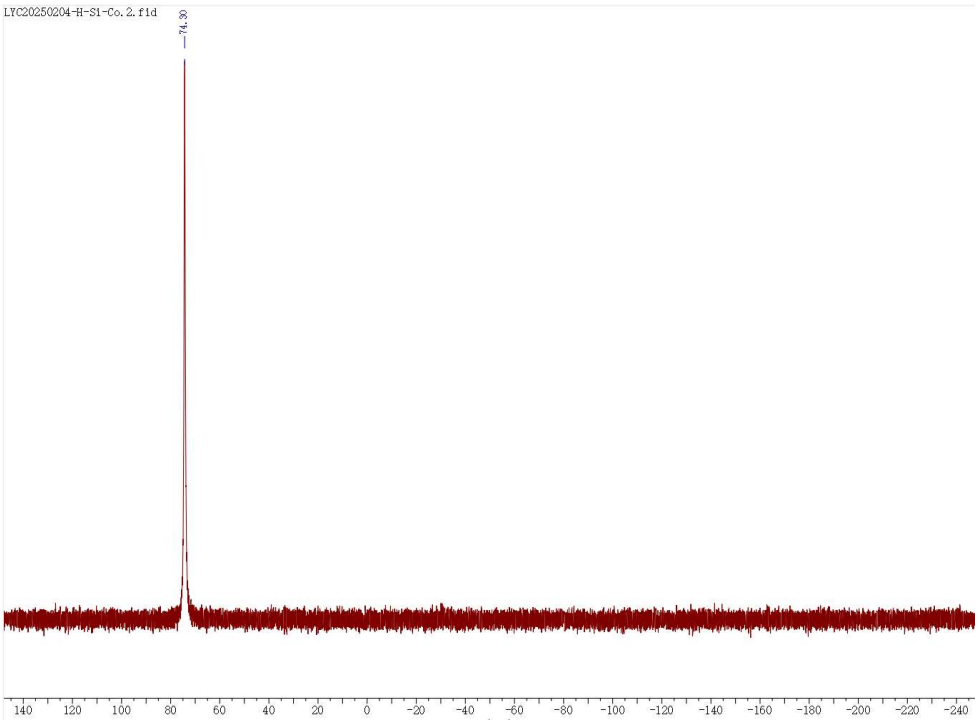

Figure S10-2. ^{31}P NMR (162 MHz, CD_2Cl_2) for compound **H-Si-Co**.

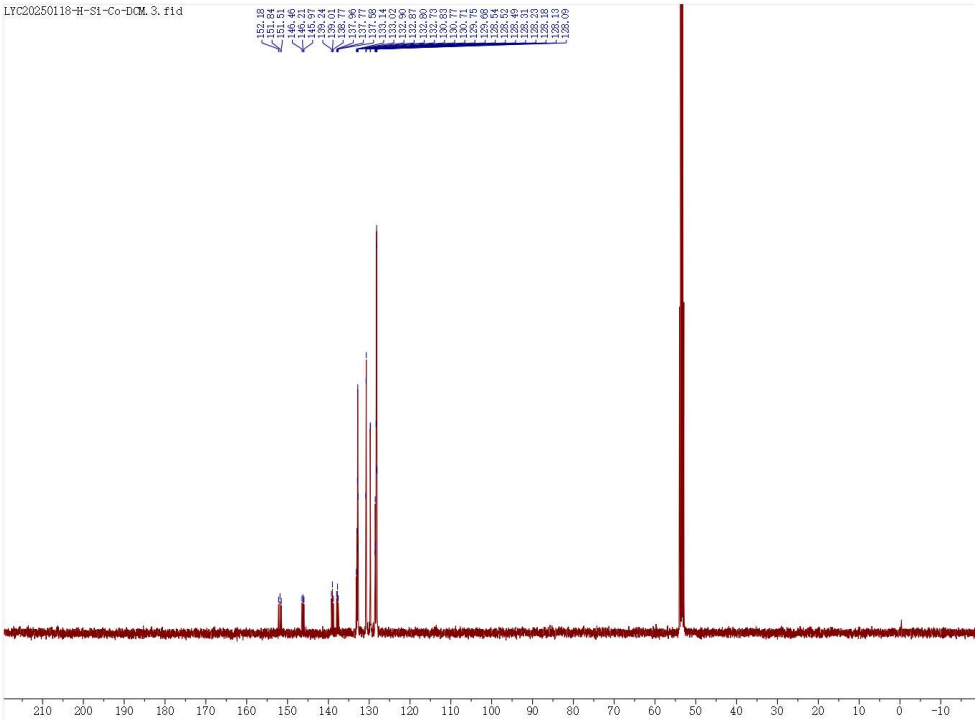

Figure S10-3. ^{13}C NMR (101 MHz, CD_2Cl_2) for compound **H-Si-Co**.

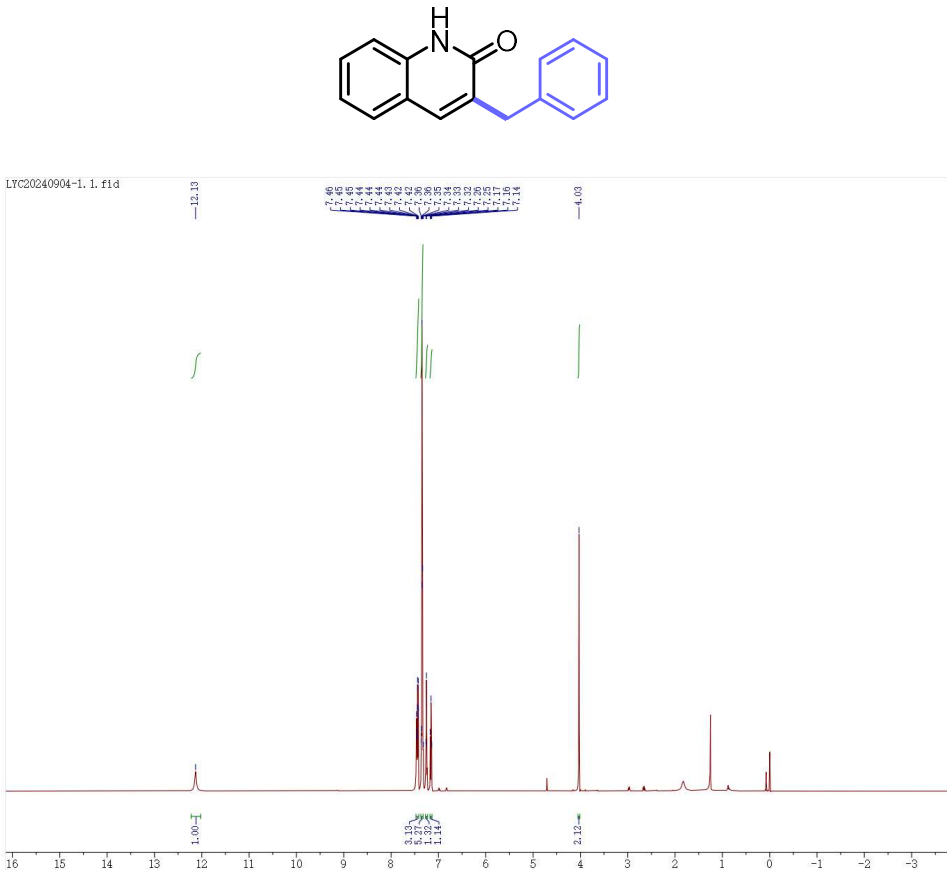

Figure S11-1. ^{1}H NMR (500 MHz, $CDCl_3$) for compound **7c**.

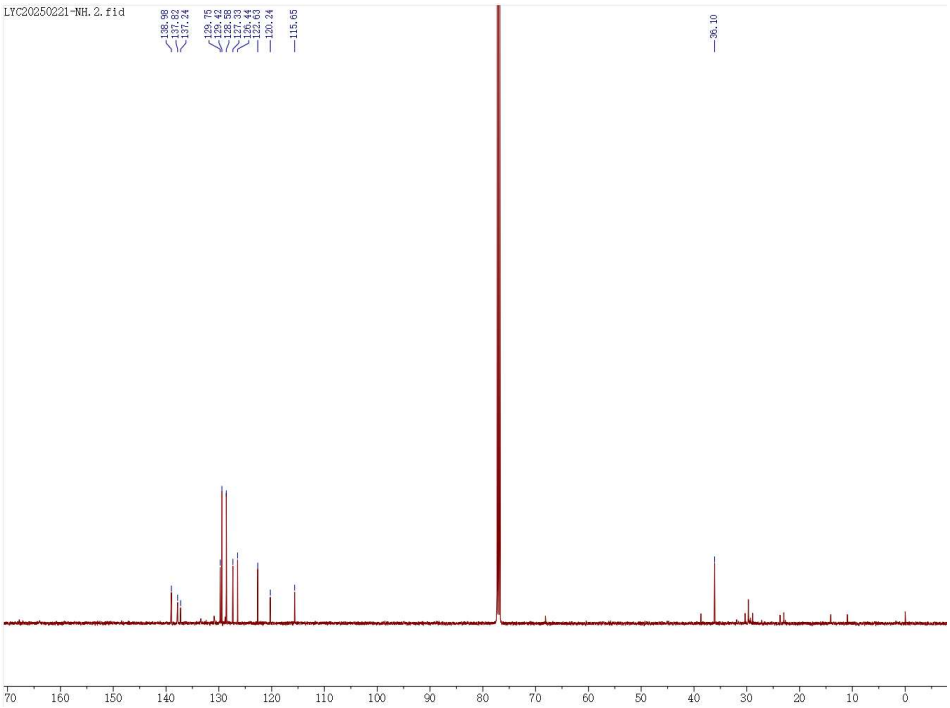

Figure S11-2. ^{13}C NMR (126 MHz, $CDCl_3$) for compound **7c**.

8. HRMS spectra of compounds

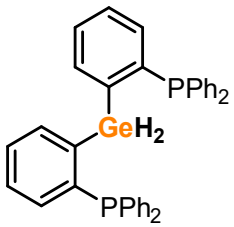

3

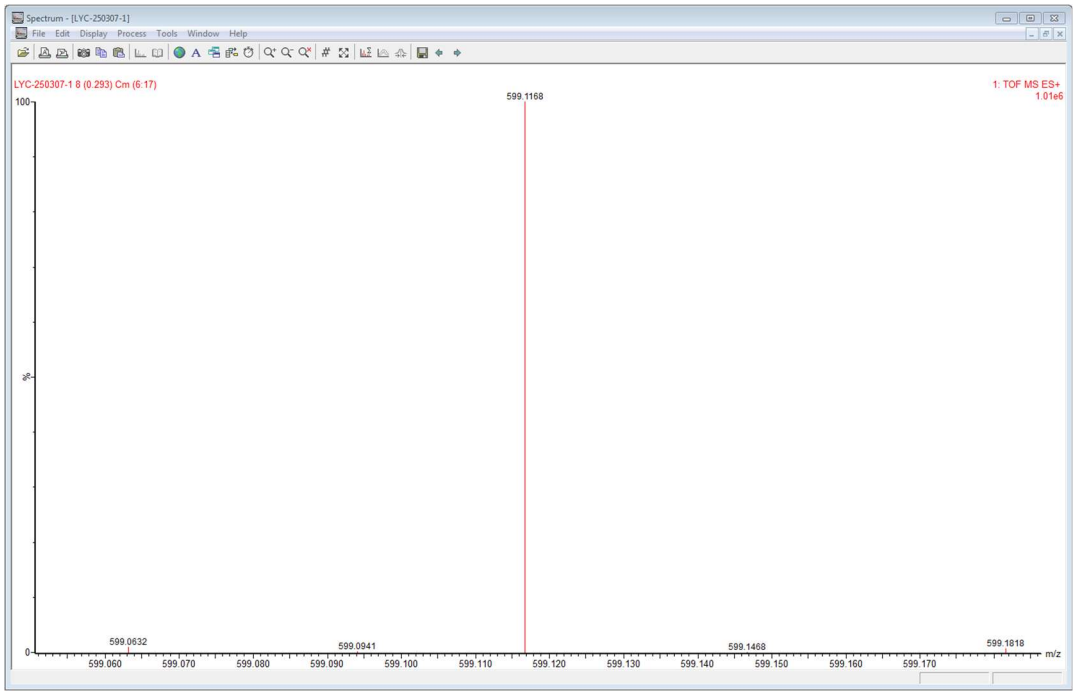

Figure S12-1. HRMS spectra for compound **3**.

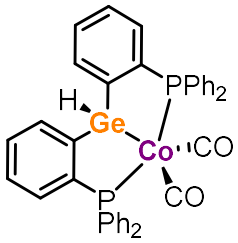

4

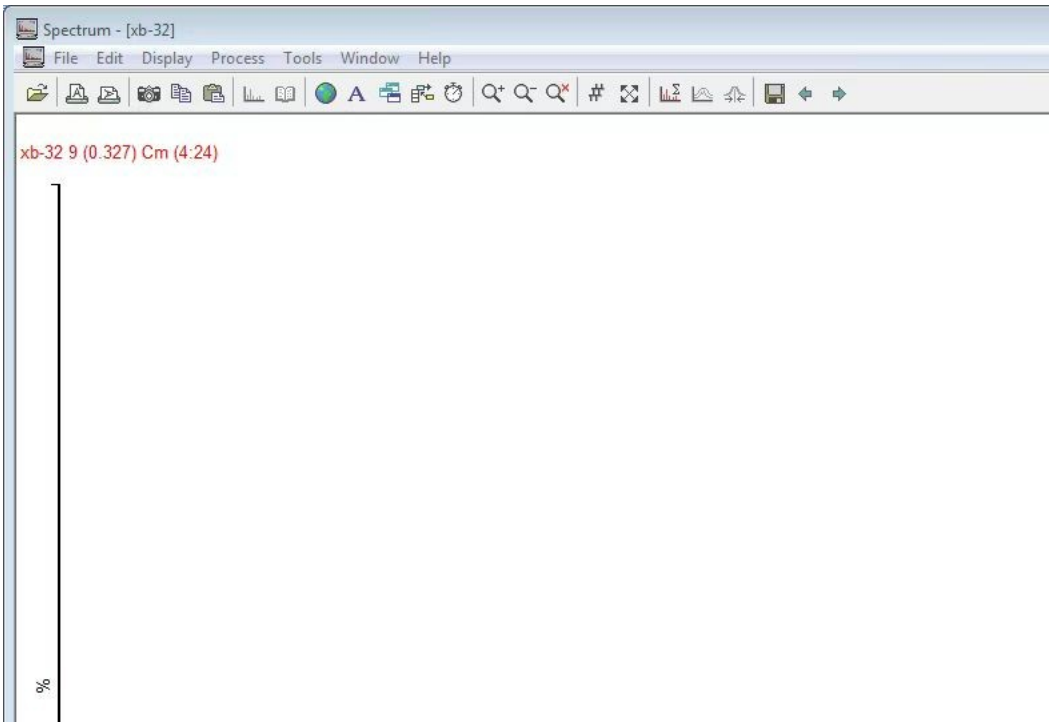

Figure S12-2. HRMS spectra for compound **4**.

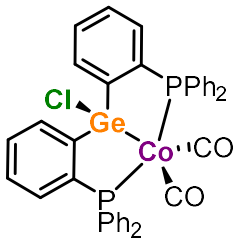

5

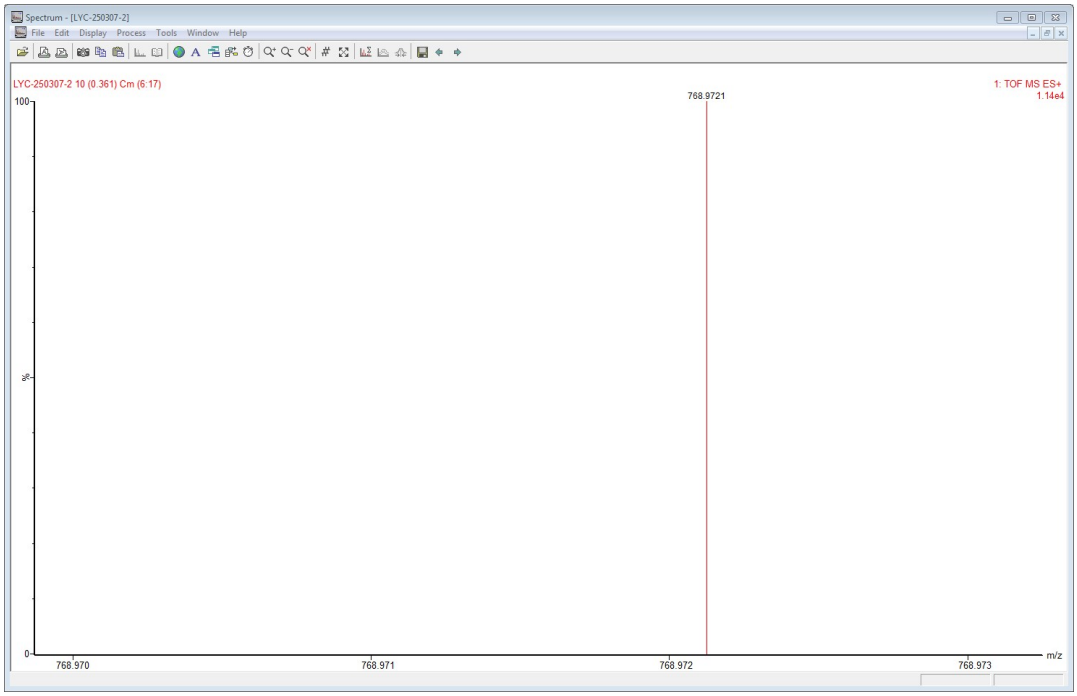

Figure S12-3. HRMS spectra for compound **5**.

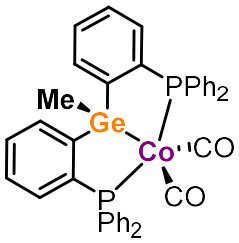

6

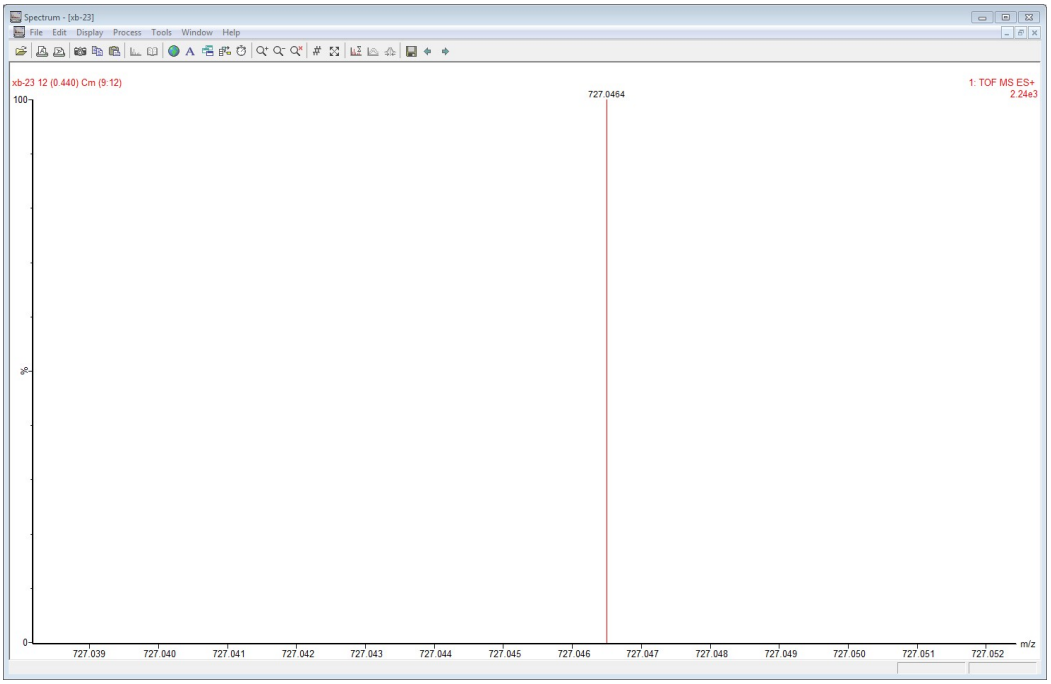

Figure S12-4. HRMS spectra for compound **6**.

9. IR spectra of compounds

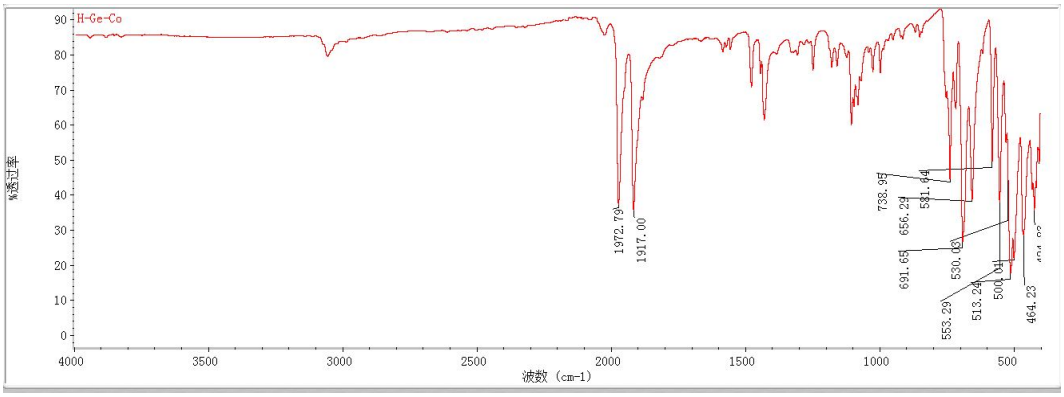

Figure S13-1. ATR-IR spectra for compound **4**.

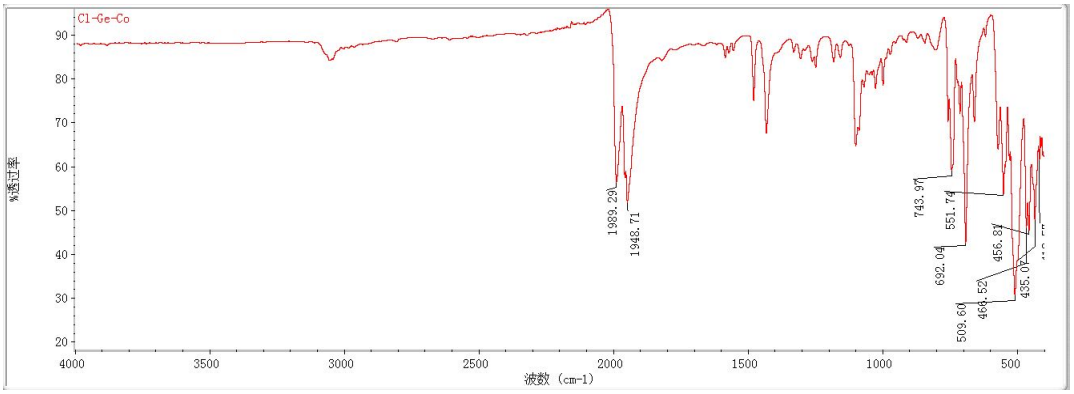

Figure S13-2. ATR-IR spectra for compound **6**.

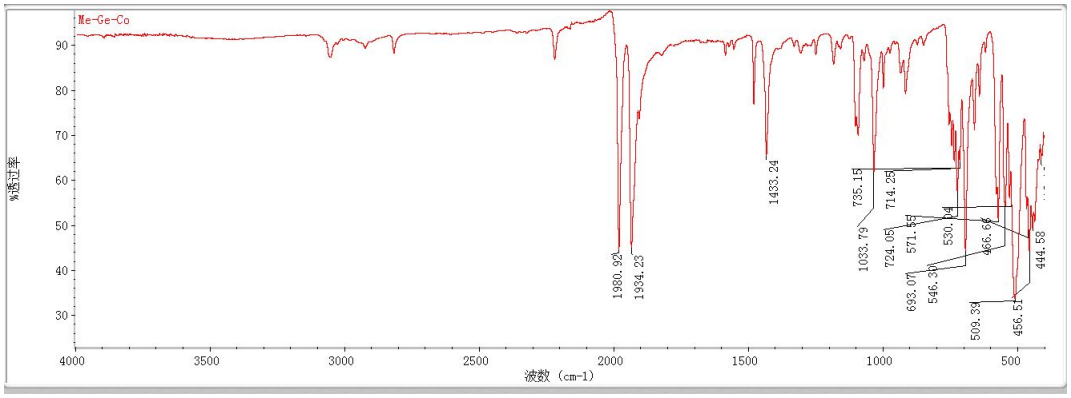

Figure S13-3. ATR-IR spectra for compound **6**.

10. Crystal structure determinations

A summary of the fundamental crystal and refinement data is provided below. Atomic coordinates, anisotropic displacement parameters, as well as bond lengths and angles can be found in the CIF files, which have been deposited in the Cambridge Crystallographic Data Centre under the accession numbers CCDC **2426452-2426456**. These data can be obtained free of charge from the Cambridge Crystallographic Data Centre via www.ccdc.cam.ac.uk/data_request/cif.

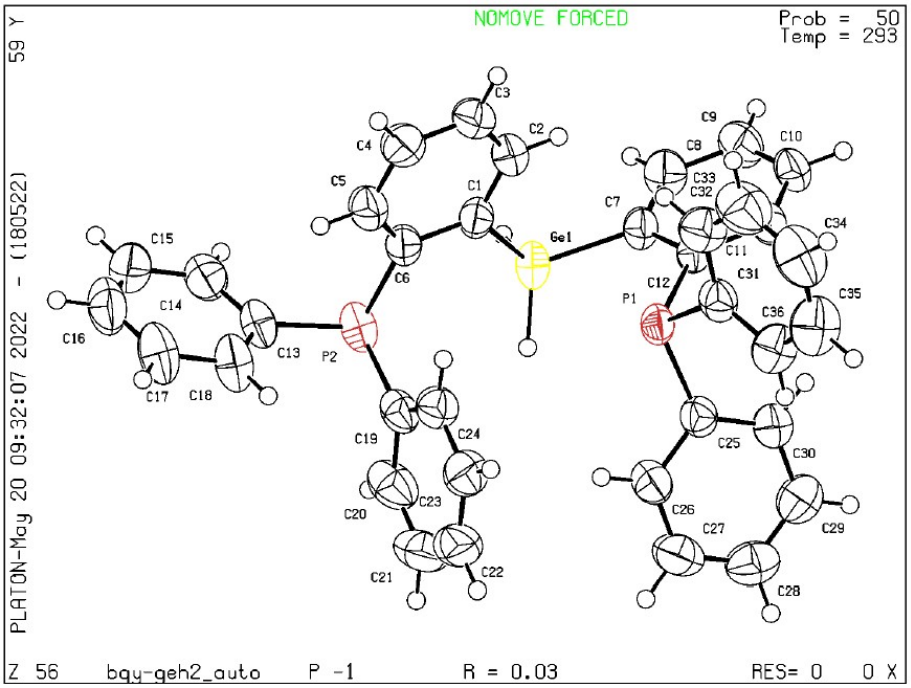

Figure S14-1-1. X-ray structure of compound **3 (CCDC 2426453)**

Table S6-1. Crystal data and structure refinement for compound **3**

Identification code	Compound **3**
Empirical formula	$C_{36}H_{30}GeP_2$
Formula weight	597.13
Temperature/K	293(2)
Crystal system	triclinic
Space group	P-1
a/Å	11.0280(4)
b/Å	12.8596(4)
c/Å	12.8744(3)
α/°	95.058(2)
β/°	113.143(3)
γ/°	108.781(3)
Volume/Å^3	1540.37(9)
Z	2
ρ_{calc}g/cm^3	1.287
μ/mm^{-1}	2.494

F(000)	616.0
Crystal size/mm^3	0.25 × 0.23 × 0.22
Radiation	Cu Kα (λ = 1.54184)
2Θ range for data collection/°	7.492 to 145.98
Index ranges	-13 ⩽ h ⩽ 13, -15 ⩽ k ⩽ 12, -12 ⩽ l ⩽ 15
Reflections collected	10875
Independent reflections	5969 [R_{int} = 0.0186, R_{sigma} = 0.0251]
Data/restraints/parameters	5969/1/361
Goodness-of-fit on F^2	1.040
Final R indexes [I>=2σ (I)]	R_1 = 0.0300, wR_2 = 0.0833
Final R indexes [all data]	R_1 = 0.0325, wR_2 = 0.0858
Largest diff. peak/hole / e $Å^{-3}$	0.26/-0.25

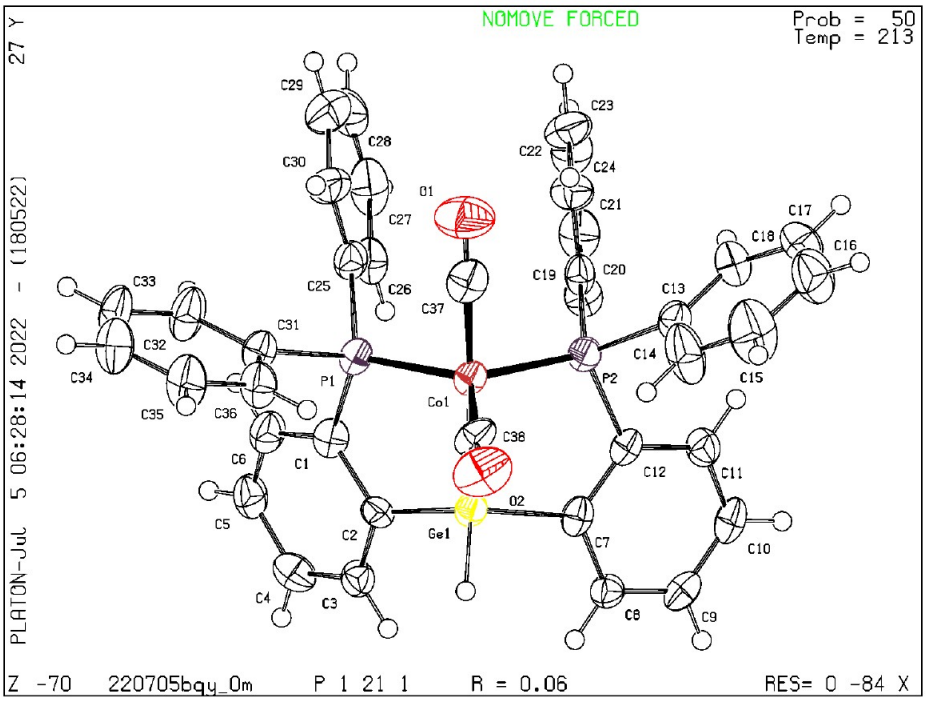

Figure S14-2-1. X-ray structure of compound **4 (CCDC 2426454)**

Table S6-2. Crystal data and structure refinement for compound **4**

Identification code	Compound **4**
Empirical formula	$C_{38}H_{29}CoGeO_2P_2$
Formula weight	711.07
Temperature/K	213.00
Crystal system	monoclinic
Space group	$P2_1$
a/Å	10.4565(5)
b/Å	14.8378(7)
c/Å	10.8171(5)
α/°	90
β/°	93.354(3)
γ/°	90
Volume/Å^3	1675.41(14)
Z	2
ρ_{calc}g/cm^3	1.410
μ/mm^{-1}	4.208
F(000)	724.0

Crystal size/mm^3	0.07 × 0.07 × 0.05
Radiation	GaKα (λ = 1.34139)
2Θ range for data collection/°	7.122 to 110.006
Index ranges	-12 ⩽ h ⩽ 12, -15 ⩽ k ⩽ 18, -13 ⩽ l ⩽ 13
Reflections collected	15283
Independent reflections	5798 [R_{int} = 0.0784, R_{sigma} = 0.0858]
Data/restraints/parameters	5798/1/366
Goodness-of-fit on F^2	1.007
Final R indexes [I>=2σ (I)]	R_1 = 0.0601, wR_2 = 0.1515
Final R indexes [all data]	R_1 = 0.0775, wR_2 = 0.1636
Largest diff. peak/hole / e $Å^{-3}$	1.72/-1.11
Flack parameter	0.186(13)

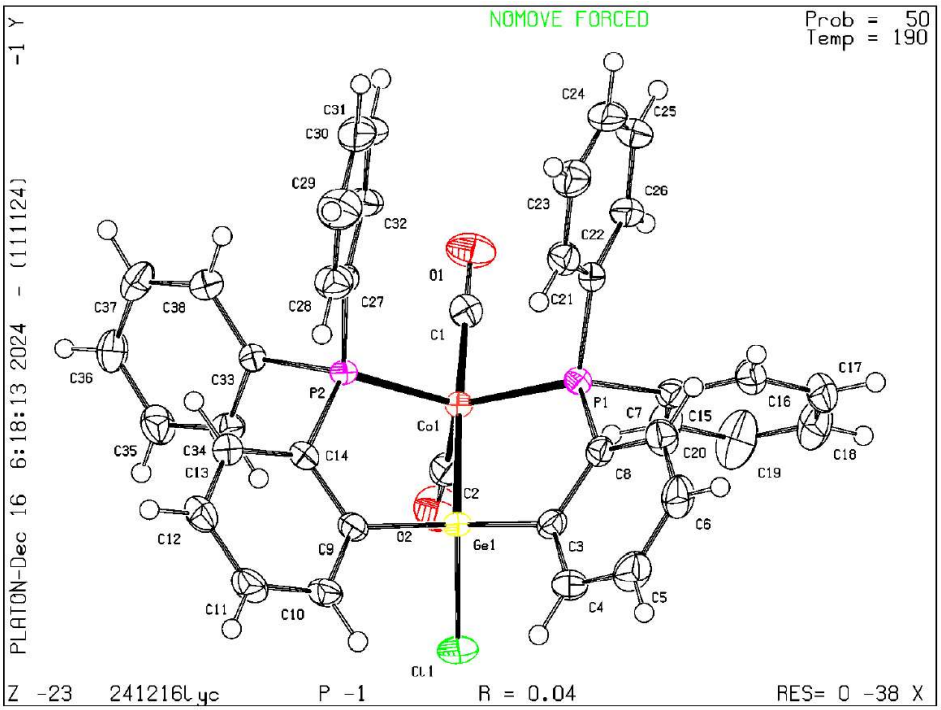

Figure S14-3-1. X-ray structure of compound **5 (CCDC 2426456)**

Table S6-3. Crystal data and structure refinement for compound **5**

Identification code	Compound **5**
Empirical formula	$C_{38}H_{28}ClCoGeO_2P_2$
Formula weight	745.51
Temperature/K	190
Crystal system	triclinic
Space group	P-1
a/Å	10.7973(5)
b/Å	11.7778(6)
c/Å	14.3651(7)
α/°	89.199(2)
β/°	83.702(2)
γ/°	87.712(2)
Volume/Å^3	1814.23(15)
Z	2
ρ_{calc}g/cm^3	1.365
μ/mm^{-1}	1.478

F(000)	756.0
Crystal size/mm^3	0.17 × 0.17 × 0.05
Radiation	MoKα (λ = 0.71073)
2Θ range for data collection/°	4.994 to 56.888
Index ranges	-14 ⩽ h ⩽ 14, -14 ⩽ k ⩽ 15, -19 ⩽ l ⩽ 19
Reflections collected	46932
Independent reflections	9076 [R_{int} = 0.0752, R_{sigma} = 0.0560]
Data/restraints/parameters	9076/0/406
Goodness-of-fit on F^2	0.985
Final R indexes [I>=2σ (I)]	R_1 = 0.0410, wR_2 = 0.1133
Final R indexes [all data]	R_1 = 0.0604, wR_2 = 0.1231
Largest diff. peak/hole / e $Å^{-3}$	0.41/-0.62

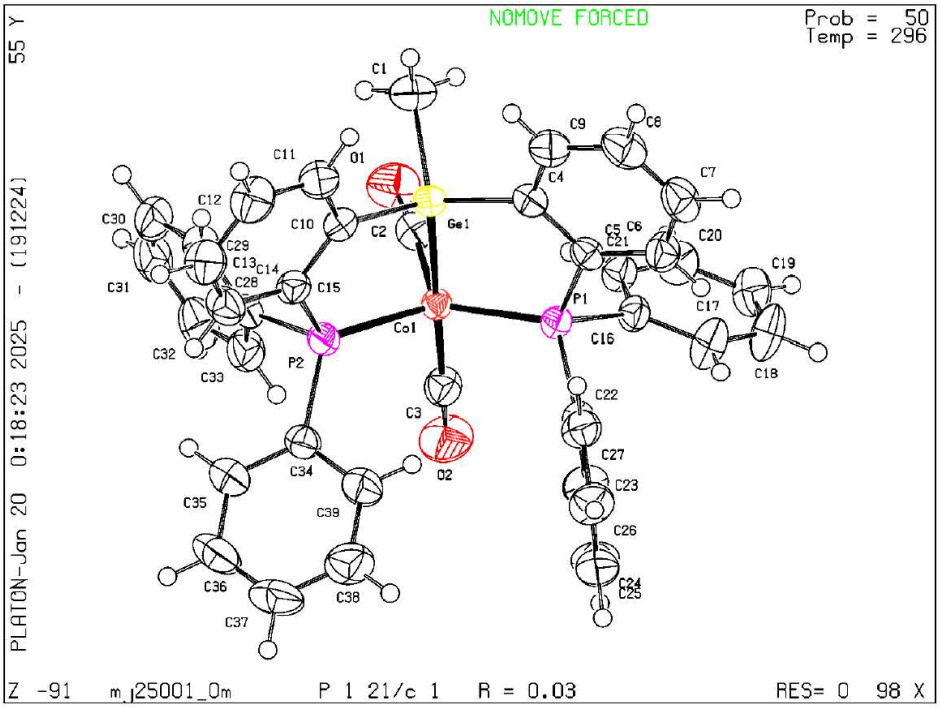

Figure S14-4-1. X-ray structure of compound **6 (CCDC 2426455)**

Table S6-4. Crystal data and structure refinement for compound **6**.

Identification code	Compound **6**
Empirical formula	$C_{39}H_{31}CoGeO_2P_2$
Formula weight	725.10
Temperature/K	296
Crystal system	monoclinic
Space group	$P2_1/c$
a/Å	10.2474(4)
b/Å	13.9407(4)
c/Å	23.4568(9)
α/°	90
β/°	99.028(2)
γ/°	90
Volume/Å^3	3309.4(2)
Z	4
ρ_{calc}g/cm^3	1.455
μ/mm^{-1}	4.268

F(000)	1480.0
Crystal size/mm^3	0.17 × 0.17 × 0.05
Radiation	GaKα (λ = 1.34139)
2Θ range for data collection/°	6.438 to 109.914
Index ranges	-12 ⩽ h ⩽ 11, -17 ⩽ k ⩽ 16, -28 ⩽ l ⩽ 28
Reflections collected	45084
Independent reflections	6293 [R_{int} = 0.0601, R_{sigma} = 0.0395]
Data/restraints/parameters	6293/0/407
Goodness-of-fit on F^2	1.013
Final R indexes [I>=2σ (I)]	R_1 = 0.0327, wR_2 = 0.0681
Final R indexes [all data]	R_1 = 0.0513, wR_2 = 0.0750
Largest diff. peak/hole / e Å^{-3}	0.28/-0.38

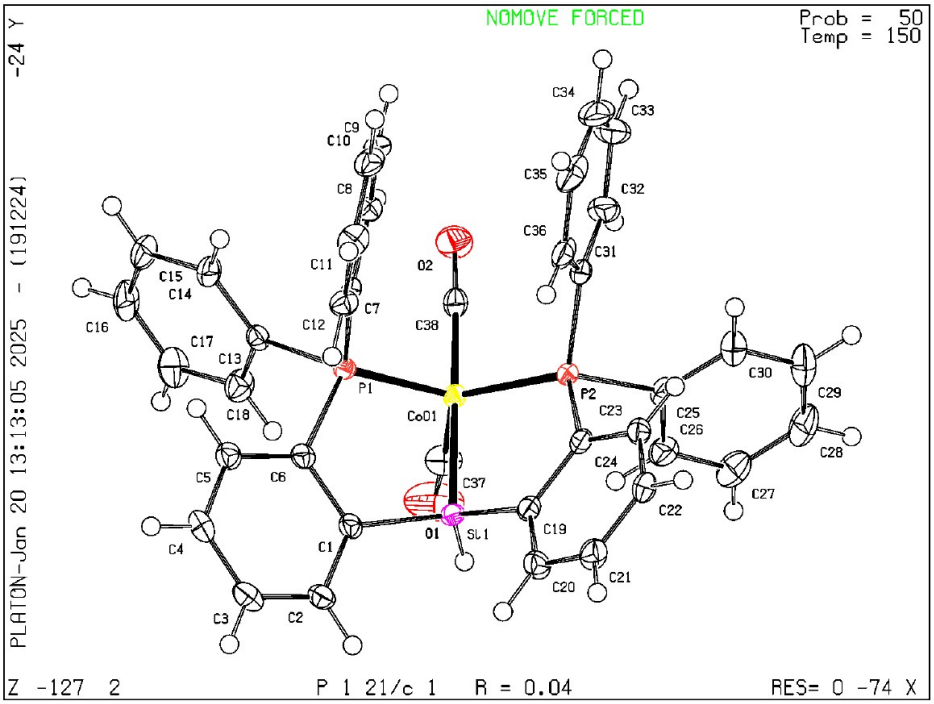

Figure S14-5-1. X-ray structure of compound **H-Si-Co**

Table S6-5. Crystal data and structure refinement for compound **H-Si-Co**

Identification code	Compound **H-Si-Co**
Empirical formula	$C_{38}H_{29}CoO_2P_2Si$
Formula weight	666.57
Temperature/K	120
Crystal system	monoclinic
Space group	$P2_1/c$
a/Å	17.2273(5)
b/Å	9.2892(2)
c/Å	20.4526(7)
α/°	90
β/°	103.117(3)
γ/°	90
Volume/Å^3	3187.59(16)
Z	4
ρ_{calc}g/cm^3	1.389
μ/mm^{-1}	5.794
F(000)	1376.0

Crystal size/mm^3	0.15 × 0.12 × 0.1
Radiation	Cu Kα (λ = 1.54186)
2Θ range for data collection/°	10.546 to 139.474
Index ranges	-20 ⩽ h ⩽ 17, -11 ⩽ k ⩽ 8, -24 ⩽ l ⩽ 21
Reflections collected	23110
Independent reflections	5852 [R_{int} = 0.0650, R_{sigma} = 0.0507]
Data/restraints/parameters	5852/0/397
Goodness-of-fit on F^2	1.000
Final R indexes [I>=2σ (I)]	R_1 = 0.0396, wR_2 = 0.0999
Final R indexes [all data]	R_1 = 0.0489, wR_2 = 0.1040
Largest diff. peak/hole / e $Å^{-3}$	0.74/-0.62

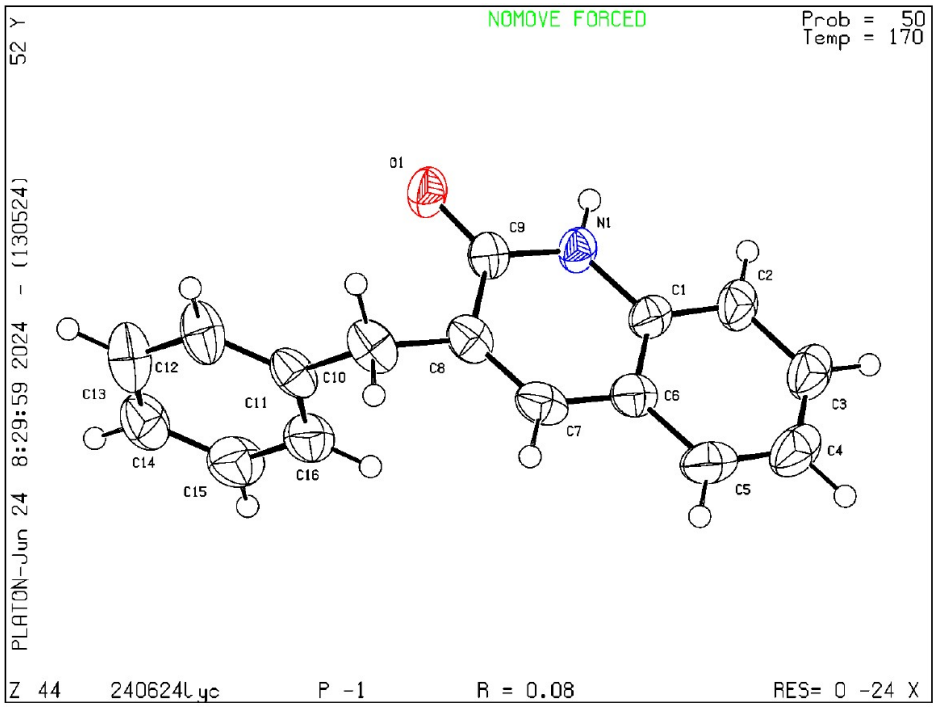

Figure S14-6-1. X-ray structure of compound **7c (CCDC 2426452)**

Table S6-6. Crystal data and structure refinement for compound **7c**

Identification code	Compound **7c**
Empirical formula	$C_{16}H_{13}NO$
Formula weight	235.27
Temperature/K	170.00
Crystal system	triclinic
Space group	P-1
a/Å	5.6306(7)
b/Å	10.8781(14)
c/Å	11.2166(16)
α/°	116.604(5)
β/°	95.399(5)
γ/°	96.893(5)
Volume/Å^3	601.32(14)
Z	2
ρ_{calc}g/cm^3	1.299
μ/mm^{-1}	0.408
F(000)	248.0

Crystal size/mm^3	0.17 × 0.17 × 0.05
Radiation	GaKα (λ = 1.34139)
2Θ range for data collection/°	7.778 to 109.832
Index ranges	-6 ⩽ h ⩽ 6, -13 ⩽ k ⩽ 12, -13 ⩽ l ⩽ 13
Reflections collected	6029
Independent reflections	2259 [R_{int} = 0.0858, R_{sigma} = 0.0925]
Data/restraints/parameters	2259/0/164
Goodness-of-fit on F^2	1.042
Final R indexes [I>=2σ (I)]	R_1 = 0.0761, wR_2 = 0.1882
Final R indexes [all data]	R_1 = 0.1353, wR_2 = 0.2341
Largest diff. peak/hole / e $Å^{-3}$	0.29/-0.28

11. References

1. J. Zhang, B. J. Foley, N. Bhuvanesh, J. Zhou, D. E. Janzen, M. T. Whited and O. V. Ozerov, *Organometallics*, 2018, **37**, 3956-3962.
2. H. Ahmed, B. Ghosh, S. Breitenlechner, M. Feßner, C. Merten and T. Bach, *Angew. Chem. Int. Ed.*, 2024, **63**, e202407003.
3. H. Tian, C.-Y. Ding, R.-Z. Liao, M. Li and C. Tang, *J. Am. Chem.Soc.*, 2024, **146**, 11801-11810.
4. K.-N. T. Tseng, J. W. Kampf and N. K. Szymczak, *ACS Catalysis*, 2015, **5**, 5468-5485.
5. I. Borthakur, A. Sau and S. Kundu, *Coord. Chem. Rev.*, 2022, **451**, 214257.